Am J Physiol Regul Integr Comp Physiol 284: R835–R852, 2003.
First published November 7, 2002; 10.1152/ajpregu.00228.2002.

A nonlinear compartmental model of Sr metabolism. II. Its physiological relevance for Ca metabolism

J. F. STAUB,[1] E. FOOS,[2] B. COURTIN,[1] R. JOCHEMSEN,[2] AND A. M. PERAULT-STAUB[1]
[1]*Unité Mixte de Recherches 7052 Centre National de la Recherche Scientifique, Laboratoire de Recherches Orthopédiques, Faculté de Médecine Lariboisière-St-Louis, 75010 Paris; and* [2]*Institut de Recherches Internationales Servier, Courbevoie, France*

Submitted 22 April 2002; accepted in final form 25 October 2002

Staub, J. F., E. Foos, B. Courtin, R. Jochemsen, and A. M. Perault-Staub. A nonlinear compartmental model of Sr metabolism. II. Its physiological relevance for Ca metabolism. *Am J Physiol Regul Integr Comp Physiol* 284: R835–R852, 2003. First published November 7, 2002; 10.1152/ajpregu.00228.2002.—We have studied the peculiarities of the nonlinear compartmental model for human Sr metabolism (Staub JF, Foos E, Courtin B, Jochemsen R, and Perault-Staub AM. *Am J Physiol Regul Integr Comp Physiol* 284: R819–R834, 2003), including its physiological reliability in the context of Sr-Ca similarity-dissimilarity. We found it to be relevant to Ca metabolism, except for discrimination against Sr relative to Ca at urinary and intestinal levels. The main findings are as follows: *1*) the saturable part of intestinal absorption, shared by Sr and Ca, does not seem to be responsible for the discrimination of the transcellular pathway; *2*) although there is little discrimination in bone, the physicochemical behaviors of Sr and Ca at the bone surface differ, at least quantitatively; and *3*) Sr behaves as a "tracer" for Ca metabolic pathways and, under non-steady-state conditions, can also reveal self-regulatory processes. It is suggested that they depend on Ca^{2+} (cationic)-sensing receptors that are apparently more sensitive to Sr than to Ca. Acting on gastrointestinal and osteoblast lineage cells, these slow processes might contribute to adaptive, rather than homeostatic, regulation of Ca metabolism. Understanding these features could help clarify the pharmacological and therapeutic effects of oral Sr.

strontium administration; calcium-strontium discrimination; self-regulatory process; calcium (cationic)-sensing receptor

IN THE ABSENCE OF EVIDENCE for a physiological role for Sr, the biological interest in this mineral and its metabolism was focused on analogies and discrepancies with Ca^{2+} as its closest divalent cation in the periodic table and the essential mineral in numerous key extracellular and intracellular processes. Sr and Ca are members of the alkaline earth series, with comparable features of cation chemistry (ionic radius, charge-to-size ratio, high coordination number, and H_2O exchange) (46). Thus they show physicochemical similarities in their interactions with organic or inorganic components. These similarities are such that the major metabolic pathways of both cations, intestinal absorption, deposition in and removal from bone, and excretion in urine and feces, are believed to involve identical processes. However, in vivo and in vitro kinetic studies, often using a tracer radionuclide of Sr^{2+} and Ca^{2+} (27, 36), have revealed, at least quantitatively, behavioral differences at gastrointestinal (GI), renal, and, possibly, bone levels (10, 42). They have been interpreted in terms of discrimination between Sr and Ca (44). Globally, retention of Ca relative to Sr is favored at the organism level.

Physicochemical analytic studies have shown that synthetic hydroxyapatite (HA), with partial substitution of Ca^{2+} by Sr^{2+} into the crystal lattice, can be produced from calcium phosphate-supersaturated aqueous solutions containing Sr^{2+}, the level of discrimination against Sr^{2+} relative to Ca^{2+} being directly dependent on the rate of crystal growth and the associated crystal perfection (24, 30). Recently, Sr^{2+} in solution was described as easily adsorbed at the crystal surface and as inhibiting the rates of HA crystal growth and dissolution (9). In vivo data indicate that Sr^{2+} can be incorporated into biological apatite (5, 12), with possible limitation in the number of substitutions.

For situations in which cations interact with organic components, the behavioral differences between Ca and Sr may be analyzed in terms of the physicochemical, stereochemical, and structural characteristics of the organic species, i.e., from nearly no difference between ion reactivities to a nearly complete specificity for Ca as a result of the small difference between Ca and Sr chemistry.

Among the main factors involved in discrimination between Sr and Ca are their relative abundance and availability in the natural environment (46). Sr is a trace element, whereas Ca is a macronutrient. Their concentrations in biological fluids also differ greatly. There are extracellular fluids with millimolar concentrations of Ca and micromolar concentrations of Sr. The very high extracellular Ca-to-Sr molar ratio means

Address for reprint requests and other correspondence: J. F. Staub, UMR 7052 Centre National de la Recherche Scientifique, Laboratoire de Recherches Orthopédiques, Faculté de Médecine Lariboisière-St-Louis, 10 Ave. de Verdun, 75010 Paris, France (E-mail: staub@ccr.jussieu.fr).

The costs of publication of this article were defrayed in part by the payment of page charges. The article must therefore be hereby marked "*advertisement*" in accordance with 18 U.S.C. Section 1734 solely to indicate this fact.

that Sr cannot significantly compete with Ca under physiological conditions; therefore, there has been little need for selection, during evolution, of mechanisms specific for Ca, rather than Sr. In vitro experiments confirm this. Sr^{2+} can replace Ca^{2+} in activating the parathyroid Ca^{2+}-sensing receptor (PCaR) (25) at a concentration that is twice that needed for Ca^{2+}. Similarly, the apical Ca^{2+} channels isolated from intestine (31) and kidney (41) are also permeable to Sr^{2+}, with higher apparent permeability for Ca^{2+} than for Sr^{2+}. However, the intracellular fluid contains 0.1 μM free Ca^{2+} (Ca_i) and Ca_i is an important second messenger for numerous cellular processes (e.g., proliferation, differentiation, apoptosis, and activity). Inasmuch as Sr is not as effectively regulated as Ca_i, their intracellular concentrations might be similar, hence, the requirement for high specificity for Ca by most intracellular proteins influencing resting Ca_i and Ca_i signaling and regulatory mechanisms. For instance, Sr^{2+} is 600-fold less potent than Ca^{2+} in causing calmodulin-induced inhibition of liver inositol trisphosphate-induced Ca^{2+} release, probably because Sr^{2+} binds 30 times less well than Ca^{2+} to calmodulin (29).

This high degree of discrimination against Sr relative to Ca for vital intracellular functions is likely the reason for hypocalcemia and/or hypocalcified bone and the decrease in 1,25-dihydroxyvitamin D synthesis, which are the first manifestations of Sr administration, only if there is a drastic increase in plasma Sr concentration. Nevertheless, plasma Sr concentration can be dose dependently increased ≥100-fold over a large range of Sr salt administration, while a molar Ca-to-Sr ratio higher than unity is always maintained. This has no apparent toxic effect and causes no significant change in plasma Ca concentration or in calcitropic hormones (17, 26).

We have reported the development of a nonlinear compartmental model for human Sr metabolism (39). In contrast to most mathematical analyses of Sr kinetics, our model focuses on Sr metabolism per se, postponing its comparison with Ca metabolism. Because it is based on non-steady-state kinetic data, it includes several nonlinearities that must be interpreted to validate our model. The primary concern of this work is to study, within the context of the Sr-Ca similarity-dissimilarity outlined above, the relevance of the model to Ca metabolism and to yield and illustrate, using model refinements, suitable explanations about the identified nonlinearities and their role in the homeostatic and/or adaptive regulation of this metabolism.

NONLINEAR COMPARTMENTAL MODEL

Briefly, the compartmental model described previously (39) was based mainly on plasma Sr concentration kinetic data collected in postmenopausal women given twice-daily oral doses of Sr (S-12911, Institut de Recherches Internationales Servier). These non-steady-state data were obtained for four doses of Sr (1.95, 3.89, 7.78, and 15.57 mmol/day) and included the increase in plasma Sr concentration during Sr administration (AdP, the first 25 days) and its decrease after cessation of treatment [postadministration period (PAdP), the other consecutive 27 days]. The plasma Sr kinetics and the fit to these experimental data obtained at the end of model building have been described previously (Fig. 1 in Ref. 39).

The model consists of two distinct, but interdependent, compartmental systems (Fig. 1).

System 1 is directly concerned with Sr metabolism and includes seven compartments describing whole body Sr and its relations to the surrounding milieu. These compartments are organized into three subsystems. *1*) The GI tract consists of two compartments (*compartments 4* and *5*): one (*compartment 4*) accepts the Sr from food (and the oral Sr administration), and the other (*compartment 5*) is associated with the irreversible excretion of Sr in the feces and the bidirectional transfer of Sr to (intestinal absorption) or from (endogenous intestinal secretion) the internal distribution pool (IDP) via *compartment 1*. *2*) The bone subsystem has three compartments connected to *compartment 1* through bidirectional (*compartments 2* and *3*) or unidirectional (*compartment 6*) relations. *Compartment 6* is directly concerned with irreversible Sr movements associated with bone mineral accretion and removal. Bone formation operates from one compartment (*compartment 2*) lying between *compartment 1* and *compartment 6*. *3*) The IDP consists of two compartments. From *compartment 1*, Sr is excreted via the kidneys; *compartment 1* includes plasma and other extracellular and, probably, intracellular sectors in

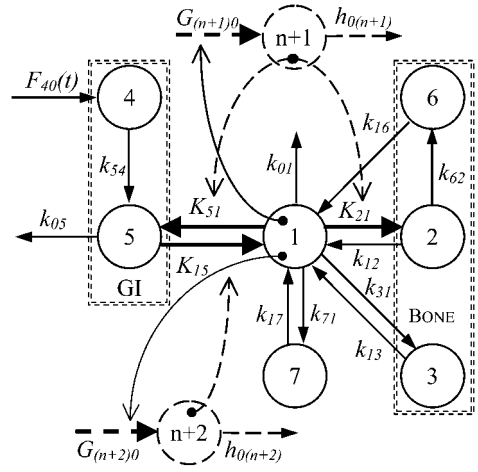

Fig. 1. Nonlinear compartmental model of Sr kinetics developed in Ref. 39. Solid lines, overall Sr metabolism (*system 1*); dashed lines, biological variables other than Sr (z variables of *system 2* interacting with *system 1*). Circles numbered 1 to 7 are kinetically distinct entities associated with Sr metabolism in bone (*compartments 2, 6*, and *3*), gastrointestinal (GI) tract (*compartments 4* and *5*), and the internal distribution pool (*compartment 1*, including plasma, and *compartment 7*). Circles numbered (n + 1) and (n + 2) are compartments representing $z_{(n+1)}$ and $z_{(n+2)}$ (*system 2*). k and K denote fractional transfer coefficients (k_{ij}) and fractional transfer functions (K_{ij}); $F(t)$ represents input pathways associated with dietary Sr and oral Sr doses. Bold arrows denote nonlinearities that are intrinsic [Michaelis-Menten (M-M) for K_{15} and Langmuir-type for K_{21}] or extrinsic due to reciprocal interactions between *system 1* and *system 2* (curved arrows). For further explanation, see APPENDIX A.

rapid equilibrium with the plasma [apparent distribution volume (V_{app}) ~40 liters]. *Compartment 7* is a rapidly exchangeable pool with no precise physiological identity. This *system 1* also contains two intrinsic nonlinearities (INL) that involve nonlinear relations to a given *system 1* compartment. These INL account for a saturable Michaelis-Menten (M-M)-type process (*Eq. A1*) involving intestinal absorption and for a Langmuir-type reaction (*Eq. A3*) involving mineral transfer from the extracellular fluids to the bone. This second nonlinearity does not behave as a simple saturable process, because it includes the inhibitory effect of one compartment that is different from the source *compartment 1*, *compartment 6,* or *compartment 3,* according to whether one refers to one or the other of both optimal models retained in the companion article (39). With reference to this inhibition variable, the optimal model here is *model L6* or *model L3*.

System 2 is relative to biological variables other than Sr [*compartments (n + 1)* and *(n + 2)*; Fig. 1]. Each extrinsic variable is associated with a one-compartment structure with an entry flow as an S-shaped growth function known as the logistic equation, affected by the Sr concentration in *compartment 1* with a high (~3 or more) cooperativity order (see *Eqs. A5* and *A6* for formulation). It acts on *system 1* through feedback modulation of some Sr transfer fluxes. The action of *system 2* on *system 1* introduces additional nonlinear functions in *system 1*, called extrinsic nonlinearities (ENL). The model includes two parameter-distinct time-explicit variables: $z_{(n+1)}$, acting on the intestinal endogenous secretion rate and on the Langmuir-type process of Sr transfer from *compartment 1* to bone *compartment 2*, and $z_{(n+2)}$, acting on the saturable intestinal Sr absorption rate.

PHYSIOLOGICAL INTERPRETATION AND MODEL REFINEMENTS

We have examined the meaning of the structure (Fig. 1) by testing the physiological reliability of the optimal models (*models L6* and *L3*) and their relevance to Ca metabolism at four levels: *1*) the initial steady state of mineral metabolism itself (for Sr and Ca), *2*) the physiological significance of intestinal and bone INL and their applicability to Ca metabolism, *3*) the kinetic and dynamic properties of the *z* logistic variables and their possible extension from dependence on Sr to dependence on Ca, and *4*) the nature of the complex interactions between INL and ENL in *system 1* and their potential meaning for the regulation of some Ca metabolic pathways and for the effects of Sr on Ca metabolism.

The relevance of the Sr model to Ca metabolism was checked with the assumption that *compartment 1* has a constant concentration of 2.5 or 1.25 mM. The experimental data (not reported) indicate that Sr has no effect on total and/or ionized plasma Ca concentration.

Model refinements were proposed to theoretically illustrate some physiological interpretations. If required, parameter estimation and a posteriori identifiability with precision of parameter values expressed as coefficient of variation (CV, in %) were carried out as described previously (39).

Initial Steady State: From Sr to Ca Metabolism

The mineral mass distribution and mean daily transfer rates for Sr and Ca metabolism can be computed for *system 1* with the assumption that Sr and Ca metabolism are in steady state under physiological conditions. As discussed elsewhere (39), with use of the set of parameter, initial condition, and V_{app} estimated from *model L6* (similar results are obtained for *model L3*), the predicted characteristics for the whole of Sr metabolism are in agreement with published data. The Sr mass in the IDP is very low compared with the predicted amount of Sr in bone (*compartment 6* contains >96% of the total body Sr mass). Estimates of the mean daily rate for ingested Sr (1.54 mg/day), urinary excretion (0.32 mg/day), and net intestinal absorption (~20% of the ingested Sr) are consistent with known Sr physiology. The main change required to apply the same model to Ca metabolism concerns *compartment 1* in *system 1*. We used the total plasma Ca concentration (Y_1 = 2,500 μM), instead of the physiological plasma Sr concentration ($y_1 \approx$ 0.5 μM). All the other model parameters were unchanged, except k_{01} was divided by 2. Indeed, the urinary clearance of Ca (2.45 ml/min) was estimated to be about one-half that of Sr (4.77 ml/min) using the Ca experimental data collected just before, during, and after the period of oral Sr administration. The extrinsic *z* variables, although kinetically influenced by Sr (and perhaps implicitly by Ca as described below), do not directly depend on the mineral species. Consequently, under physiological conditions (at *time 0*), they act identically on each fractional transfer function (FTF) that they modulate (K_{15}, K_{51}, and K_{21}; Fig. 1), regardless of the mineral metabolism concerned. Unlike a linear model, shifting *system 1* from Sr to Ca metabolism does not give obvious results, because the INL are sensitive to the absolute concentrations of the variables they involve. However, in the initial steady state, the only effective INL is the M-M function with its *compartment 5* mineral (Sr and/or Ca) concentration dependence. Indeed, according to the normalized version of the other INL, Langmuir-type nonlinearity (*Eq. A3*), the value of the transfer function from *compartment 1* to *compartment 2* is independent of the value of the inhibition variable at *time 0*.

The results presented in Table 1 show that applying *model L6* to Ca metabolism gives rise to a number of predicted theoretical values that agree with the known characteristics of Ca metabolism. With application of the same model parameters for Ca and Sr, except for the urinary excretion, the relative mass distribution of Ca within the body (IDP and bone) is similar to that of Sr. The total Ca mass is ~900 g, with >800 g in *compartment 6* and only ~30 g (3.4% of the total mass) in the other compartments. The fluxes into and out of *compartment 6* (bone mineral solid phase) give a Ca bone turnover of ~600 mg/day, 1.6 times the Ca uri-

Table 1. *Sr and Ca masses and main metabolic pathways estimated from the steady-state solution of model L6*

Predicted Characteristic	Sr	Ca
m_1 (or M_1)	2.29 mg	4.95 g
m_2 (or M_2)	3.11 mg	6.72 g
m_3 (or M_3)	2.99 mg	6.47 g
m_7 (or M_7)	5.16 mg	11.16 g
m_6 (or M_6)	386.5 mg	836.0 g
m_4 (or M_4)	0.11 mg	0.71 g
m_5 (or M_5)	0.10 mg	0.76 g
Total mass	400 mg	865.29 g
Bone turnover	0.259 mg/day	559.9 mg/day
Urinary excretion	0.32 mg/day	343.2 mg/day
Ingestion	1.54 mg/day	9.59 g/day
Intestinal absorption	20.6%	3.6%

For all parameter values and coefficients of variation of this model, see Table 4 in Ref. 39.

nary excretion (340 mg/day), with a mean residence time in *compartment 6* of ~4 yr. On the contrary, applying the GI parameter to Ca metabolism reveals a considerable discrepancy between Sr and Ca. The model predicts an unrealistic value of >9 g/day for mean Ca ingestion, whereas the net intestinal balance (340 mg/day) represents <4% of the predicted Ca daily ingestion (~96% is excreted in feces), although its absolute value is not inconsistent. This meaningless model prediction can be made realistic by reducing K_{51}, the value of the FTF linked to the return of mineral from *compartment 1* toward *compartment 5* (Fig. 2). Dividing k_{51} by 8–10 gives an expected daily Ca ingestion of ~1 g, with a net intestinal absorption >30%. This causes no change in the other properties that fit the expected processes involved in Ca metabolism of these human subjects. Thus, in addition to urinary excretion, our results suggest that some of the mechanisms influencing the bidirectional relation of the GI compartment to *compartment 1* differ quantitatively between Ca and Sr metabolism (see below).

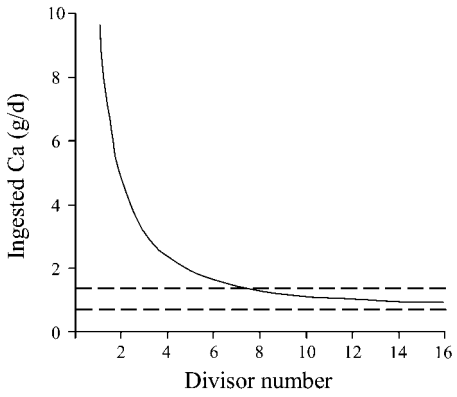

Fig. 2. Initial steady-state prediction for daily dietary Ca intake required when *model L3* is applied to Ca metabolism as a function of decreasing intestinal endogenous mineral secretion (K_{51} divided by an increasing divisor number). Dashed lines delimit the expected physiological range of daily dietary Ca intake.

GI and Bone INL

The INL include one extra assumption that may be important for the kinetic and dynamic behavior of our model, in contrast to the ENL, which depend on the time-explicit z variable. This assumption is the pseudo-steady-state hypothesis, which assumes that any intermediary step involved in a substrate-product transformation (e.g., mineral transfer from one compartment to another) is in rapid equilibrium compared with the overall transformation rates. It is possible to test the reasonableness of such an assumption (see APPENDIX B). This is important, because the INL (M-M and Langmuir) in our model are modulated by the extrinsic (time-explicit) z variables. Thus we will compare experimental data with the response of refined models, making explicit the kinetic behavior of intermediary steps neglected under the intrinsic formulation. Only after that, will we attempt any physiological interpretation of the processes of intestinal mineral absorption or mineral transfer from the extracellular fluids to bone.

Intestinal M-M-type process: Sr-Ca similarity-dissimilarity. The transfer function K_{15} from GI *compartment 5* to *compartment 1* in our model (Fig. 1) is governed by an M-M equation in addition to a simple linear process (*Eq. A1*). This kind of representation has been used to account for in vitro data on Ca intestinal absorption (45), demonstrating that the transfer of mineral from the GI compartment to extracellular fluids is the sum of two distinct processes: one is saturable and mediated by species required for the intracellular mineral transfer but present in limited amounts; the other is unsaturable and remains proportional to mineral concentration in the lumen.

Attempts to explicitly introduce the intermediary species presumably involved in the saturable carrier-mediated process (see APPENDIX B) have failed to give results that improve the fit to the experimental data or give more precise supplementary parameter values. These parameters are also high, in agreement with the rapid equilibrium (pseudo-steady-state) assumption. Thus the M-M equation seems adequate. Figure 3 illustrates the type of behavior predicted from the FTF K_{15} parameter values identified for *model L6* at *time 0*, i.e., under physiological conditions, and shows the lin-

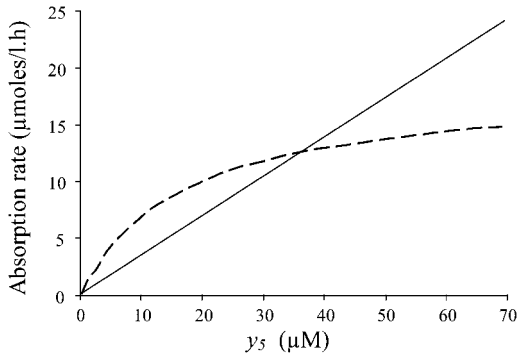

Fig. 3. Predicted dependence of linear (solid line) and nonlinear (dashed line) Sr intestinal absorption rates on *compartment 5* concentration. Values are expressed as apparent concentration.

ear and nonlinear dependence of the intestinal absorption rate on the apparent mineral concentration in *compartment 5*. The maximum rate of the saturable process, $k_{15}^2 z_{(n+2)}(0)$, can be estimated to be 21.6 mmol/day, using V_{app}, or >1.8 g/day of Sr. This value is $>10^3$ times the predicted Sr daily intake and, thus, has no reliable meaning in terms of the regulation of Sr intestinal absorption in physiological conditions. Similarly, k_{15}^3, which defines the concentration in *compartment 5,* from which the rate of transfer to *compartment 1* is half-maximal, is ~0.8 mM if the intestinal volume is assumed to be on the order of 1 liter. This millimolar estimate for k_{15}^3 is much higher than the expected physiological Sr concentration in intestinal juice. On the contrary, the maximum rate and k_{15}^3 values are quite consistent with a physiological process directly concerned with intestinal Ca absorption. The half-maximal concentration of the saturable process agrees with the mechanism of facilitated entry that dominates at low luminal Ca concentrations (38) and saturates at 0.4–1 mM (14, 31). Furthermore, the maximal daily rate for Ca, ~860 mg/day, is consistent with, but slightly lower than, the normal daily Ca intake.

Nevertheless, the discrepancy between Sr and Ca (see *Initial Steady State: From Sr to Ca Metabolism*), which is apparently linked to the amount of mineral secreted from *compartment 1* to the GI compartment, prompted us to look for a plausible biological mechanism for the bidirectional relation of the GI compartment to *compartment 1* indicated by our model. Although it is generally accepted that mineral may be secreted from extracellular fluids into the gut, there is still debate as to whether this mineral is reabsorbed by the intestine and whether Ca and Sr are secreted into the intestinal lumen via paracellular and/or transcellular routes (23). The models developed here indicate negligible fecal loss of Sr directly from *compartment 1* but significant intestinal reabsorption of endogenous Sr. This, together with the fact that k_{15}^2 and k_{51}, which describe the maximum rate of saturable absorption and the endogenous intestinal secretion, are influenced by the same kind of ENL, led us to examine a model that dissociates the transcellular and paracellular pathways and, consequently, the saturable and nonsaturable parts of intestinal absorption. We included an intermediary compartment (*compartment 1′*) between *compartments 1* and *5*, possibly representing the mineral within intestinal epithelial cells. Figure 4 shows the three assumptions: *1*) *compartment 1′* is in linear exchange with *compartment 1*, *2*) the linear part of intestinal absorption (the paracellular route) operates directly from *compartment 5* to *compartment 1,* and, thus, the fractional transfer function from *compartment 5* to the intermediary compartment, $K_{1'5}$, obeys M-M kinetics, and *3*) the transfer of mineral from the intermediary compartment to *compartment 5* and the maximum rate of the saturable process are modulated by the extrinsic variables $z_{(n+1)}$ and $z_{(n+2)}$. These assumptions allow the model response [quite identical to that obtained from the initial *model L6* (see Fig. 1 in Ref. 39)] to be correctly fit to experimental data without any significant change in parameter values other than those directly related to the intermediary compartment. However, the great inaccuracy of some parameter values precludes any quantitative interpretation of these results. Consequently, only the high turnover rate between the intermediary compartment (*compartment 1′*) and *compartment 1* and its initial value, which is much lower than that of *compartment 1,* must be pointed out. The parameters defining the saturable process did not change significantly.

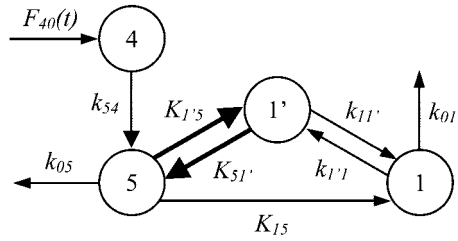

Fig. 4. Refined nonlinear compartmental substructure for GI Sr metabolism. Compartments are as shown in Fig. 1, except for intermediary *compartment 1′*, which is associated with intestinal intracellular mineral. Rate-limiting (M-M-type) process of transcellular mineral transport from GI *compartment 5* to *compartment 1* is the apical entry into epithelial cells indicated by $K_{1'5}$ that, as for $K_{51'}$, is modulated by a *z* extrinsic variable. k_{15} denotes paracellular nonsaturable (linear) intestinal absorption. See Fig. 1 legend for explanation of symbols.

Even if there is no justification from a strict modeling point of view, this model can lead to interesting physiological interpretation. In agreement with the GI model shown in Fig. 4, the first step in the transcellular process of intestinal absorption, the Ca uptake by enterocytes ($K_{1'5}$), is given as a first saturable pathway and a decisive rate-limiting step in the overall process (41). The two subsequent steps in transcellular intestinal absorption, cytosolic facilitated diffusion [calbindin(s)-dependent] and active extrusion across the basolateral membrane (via Ca^{2+}-ATPase and/or Na^+/Ca^{2+} exchanger) (45), are parts of the rapid transfer of mineral from the intermediary compartment to *compartment 1*, $k_{11'}$. Our model indicates that there are pathways opposing this process, with the transcellular transfer from *compartment 1* to *compartment 5* passing through the intermediary compartment, with the possible reabsorption of secreted mineral. This expands the regulatory potential of the GI mineral metabolism. This feature is clear, because the amount of Sr transferred by the unsaturable paracellular process (0.820 mg/day) exceeds the net balance at the intestine (0.371 mg/day) as estimated at the initial steady state from the identified parameters of the satisfactory *model L6*. In other words, the intestinal secretion of Sr (3.10 mg/day) is greater than the amount of Sr absorbed through the saturable process (2.60 mg/day), so that the net balance of the bidirectional transcellular pathway is negative (−0.503 mg/day). This explains the difficulty in applying the GI parameters to Ca metabolism. This problem can be overcome by assuming that it is the ion transfer from the intermediary compartment to *compartment 1*, by cytosolic diffusion and/or

basolateral extrusion, that discriminates against Sr, contrary to our initial suggestion that more Sr than Ca is secreted toward the lumen (see *Initial Steady State: From Sr to Ca Metabolism*). A higher value of this already high transfer coefficient, $k_{11'}$, for Ca than for Sr may reduce the steady-state value of the intermediary compartment (Ca_i concentration becoming lower than intracellular Sr concentration) and, thus, the Ca efflux from this compartment toward the lumen. For instance, daily Ca intake will be normal and there will be some endogenous Ca intestinal secretion if $k_{11'}$ is 8- to 10-fold larger. The mechanisms underlying reversibility, at least partial, of the processes involved in the mineral relations between the lumen and the intracellular milieu remain to be studied (see *An integrative mechanism for intestinal secretion of endogenous mineral*).

Bone Langmuir-type function, an Sr-specific process. The second INL is the so-called Langmuir-type function. It operates on K_{21}, the FTF related to the transfer of mineral from *compartment 1* to the major bone *compartment 6* via *compartment 2* (Fig. 1). The interpretation of the present nonlinearity differs from that of intestinal absorption, because it concerns the bone, where not only the cellular and organic components may interact with mineral, but also the various mineral physicochemical reactions may be directly responsible for the nonlinearity. For instance, the adsorption of mineral species at the surface of the bone solid phase or other deeper sites, such as ion integration or substitution inside the crystal lattice, may be saturable processes, because they depend on free sites, the number (concentration) of which may be restricted. Similarly, the reactivity of these sites may change with the composition of the liquid or the solid phase. Impurities (foreign ions) may act as solutes or as constituents of the crystal lattice and so inhibit some of the numerous steps involved in bone mineralization (1–3, 9).

As reported in APPENDIX A, the intrinsic form for this Langmuir-type nonlinearity (*Eq. A3*) is derived from a more general equation (*Eq. A4*) that anticipated complex nonlinear behavior due to a saturable process dependent on the mineral concentration of the source compartment and the inhibition by a compartment other than the source compartment. The model refinements undertaken here to clarify the physicochemical processes involved in the bidirectional transfer of mineral across the solute ions-bone solid phase interface were based on a scheme including a priori the two nonlinear components of the general equation. For this, we used a procedure similar to that reported in APPENDIX B, in which the rapid equilibrium (pseudo-steady-state assumption) of possible intermediary species, so far neglected in any intrinsic form of the Langmuir-type nonlinearity, is questioned. Obviously, the complexity of the refined structures increases: at the most, three compartments (2 for *system 1* + 1 for *system 2*) and three parameters could be added. Model refinement was also attempted to check Ca and Sr interactions in their binding to the same absorption sites as illustrated in APPENDIX C.

Conditions for numerical parameters similar to those reported previously (39) (the 4 Sr doses were considered simultaneously) were used in several models to study their ability to fit the experimental data. Indeed, the Langmuir reaction can be inhibited in various ways (APPENDIX B) and so have various compartmental representations. Nevertheless, they have several features in common. The first feature is explicit formulation of a Langmuir-type process as the first step in the transfer of mineral from *compartment 1* to the bone bulk solid phase (*compartment 6*) via *compartment 2*. An additional compartment (*compartment 1'*, called the interfacial compartment), inserted between *compartment 1* and *compartment 2*, accounts for the reversible attachment of mineral ions at particular binding sites on the bone surface (Fig. 5). This reaction may be simple adsorption and is assumed to be of first order in its dependence on the concentration of mineral ion (y_1) and free sites [$z_{(n+3)}$] for uptake. The release of mineral ions from the bone surface and the resulting recovery of free sites are proportional to the concentration of mineral bound to sites ($y_{1'}$). The second feature is inclusion of an irreversible flux from the interfacial *compartment 1'* to *compartment 2* as a second step of the mineral transfer toward bone. This transfer is believed to be related to the formation of an initial mineral ion association that is relatively unstable, because it can dissociate into solute ions (direct transfer of mineral from *compartment 2* to *compartment 1*; Fig. 5). This results in the recovery of one free site for each ion incorporated. According to our model, the extrinsic logistic $z_{(n+1)}$ function (see below for its physiological interpretation) modulates the rates of mineral incorporation and the recovery of the associated free sites.

Introduction of the Langmuir reaction plus an inhibition into the model results in a satisfactory fit, whatever the type of inhibition chosen. However, a posteri-

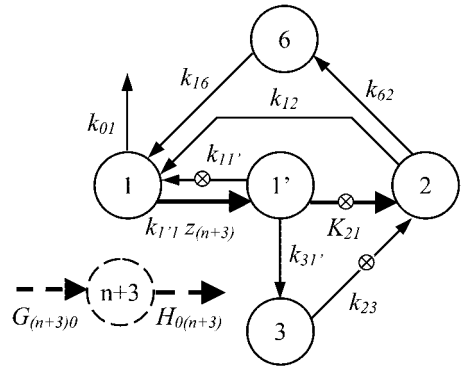

Fig. 5. Refined nonlinear compartmental substructure for bone Sr metabolism. Explicit representation of mineral adsorption at the bone surface is shown as the first reversible step of Sr (and Ca) incorporation into the bone solid phase. *System 2 compartment (n + 3)* characterizes free adsorption sites. *Compartment 1* includes plasma. Intermediary *compartments 1'* and *3* are associated with mineral bound to adsorption sites and *compartments 2* and *6* with mineral incorporated into the first and deep layers of bone solid phase. See Fig. 1 legend for explanation of symbols. ⊗, Fractional transfer associated with recovery of free sites. *Compartment 3* acts as a noncompetitive inhibitor. For further explanation, see APPENDIX B.

ori identifiability study reveals that some of the identified parameter values are very inaccurate. Only when the inhibition is noncompetitive do the structures give reasonably precise parameter values (CV < 100%). Interestingly, under these conditions, few additional compartments and parameters are required, because *compartment 3*, in linear relation to *compartment 1* in the initial structure (Fig. 1), is no longer required. It seems that the turnover rate between *compartment 1* and the interfacial *compartment 1′* is high enough that the kinetic effect of *compartment 3* is maintained, despite its structural translocation. For example, the bone substructure shown in Fig. 5 has *compartments 1′* and *3* in *system 1* and *compartment (n + 3)* (free site concentration) in *system 2* directly belonging to an explicit form of the Langmuir process plus a noncompetitive inhibition. We can account for the noncompetitive inhibition by assuming that *compartment 3* is produced from *compartment 1′* without recovery of free sites, with the sites recovered later when *compartment 3* supplies mineral to *compartment 2*. This last process is linear, in contrast to that providing material directly from *compartment 1′*: the mineral transfer from the interfacial *compartment 1′* to *compartment 2* is modulated by the $z_{(n+1)}$ logistic function. Under such conditions, the identified values for parameters of *system 1* (GI, IDP, and bone) and *system 2* [$z_{(n+1)}$ and $z_{(n+2)}$], other than those directly involved in the new ENL [$z_{(n+3)}$], are broadly similar to those estimated for the initial simple *models L3* and *L6*. Consequently, the predicted Sr mass distribution within the model and the transfer rate associated with the main Sr metabolic pathways are essentially identical to those at *time 0* in *models L3* and *L6*. Now, when the predicted model characteristics directly related to the inhibited Langmuir representation are taken into account, it emerges that, at the initial steady state, i.e., under physiological conditions, the turnover between *compartment 1* and the interfacial *compartment 1′* is more rapid than that of *compartment 2* ($k_{11'}/K_{21'}$ = 30.5) and very similar to that of *compartment 7*, the sole IDP compartment in linear relation to *compartment 1*. This turnover is also ~40 times higher than bone metabolism, involving *compartment 6* with its mineral transfer rates similar to bone mineral accretion and removal. Also, *compartment 3*, which describes mineral species (Sr^{2+} or small clusters such as ion pairs containing Sr) adsorbed at the bone surface, as does *compartment 1′*, resembles a relatively slowly exchanging pool of mineral bound to sites with a mean residence time ($1/k_{23}$) of ~28 days. It is the largest portion of the Sr at the liquid-solid bone interface (85% of *compartments 1′* and *3*). Finally, the estimated quantity of free sites, *compartment (n + 3)*, represents >99% of the total number of sites, with only ~1% occupied by Sr. Briefly, using the time-explicit formulation of the Langmuir-type nonlinearity, the above properties of our model seem to indicate that interfacial mineral dynamics are important in the overall process of Sr incorporation into the bone mineral solid phase.

Nevertheless, because most of these processes are also relevant to bone Ca metabolism, another model refinement was examined that accounts mainly for Ca^{2+} and Sr^{2+} interaction in their binding to the same adsorption sites at the bone surface. This study seems to be all the more appropriate, inasmuch as the identified apparent concentration of free sites is very low compared with the plasma Ca concentration. The procedure illustrated in APPENDIX C was applied to the model structure given in Fig. 5: *compartments 1* (free mineral ions), *1′*, and *3* (mineral bound to sites, with *compartment 3* related to inhibition) were considered explicitly for the Sr and Ca concentrations (*systems 1* and *I*, respectively, see APPENDIX C); *compartment (n + 3)* is common to Sr and Ca metabolism, because it represents the free adsorption sites that bind Ca and Sr.

These conditions and the *compartment 1* Ca concentration (Y_1) constant (2,500 μM) gave a satisfactory fit using the bone compartmental substructure given in Fig. 5 with the same set of parameter values for Sr and Ca ($k_{ij} = \lambda_{ij}$), except for the parameter linked to the recovery of free sites from *compartment 3* (incorporation of mineral into the first mineral solid phase, *compartment 2*). Contrary to Sr, for which k_{23} is relatively low (2.2×10^{-3} h^{-1}), λ_{23}, which defines the same transfer process, except for Ca, must be ≥10 times larger than k_{23} for the model response to fit experimental data (fit not significantly different from that obtained when Sr alone is considered or with the original satisfactory *model L3* or *L6*). This result can be easily interpreted if the processes involved in Ca dynamics at the liquid-solid bone interface are operating without inhibition of the overall process of mineral incorporation into the bone solid phase. Thus this inhibition is specific for Sr, perhaps shared with other foreign ions, but not with Ca. It seems to involve processes of Sr adsorption onto forming or growing apatite nuclei and/or onto the surface of existing bone mineral solid phase.

Unfortunately, this last Ca- and Sr-refined model is not accurate enough for some of the identified parameter values; thus a detailed examination of its properties is ruled out. Nevertheless, there was no significant variation in the set of parameter values relative to metabolic pathways other than those directly concerned in the Langmuir nonlinear expression, similar to the previous version that considered the interfacial dynamics of Sr alone. Moreover, the very low apparent concentration of free sites (~20 μM, not significantly different from zero) is probably the origin of the large inaccuracy observed on the Langmuir FTF. The reason for this seems to be that Ca occupies most of the adsorption sites in the initial steady state (~96% of the total number of sites vs. 3.5% of free sites and <0.5% of sites occupied by Sr). Besides its noncompetitive inhibitory effect, Sr acts mainly by diminishing the number of sites associated with Ca. Now, if only the competition between Ca and Sr at the binding level is considered and identical parameter values for Ca and Sr relations are assumed between *compartment 1* and the interfacial *compartment 1′*, the model predicts that the

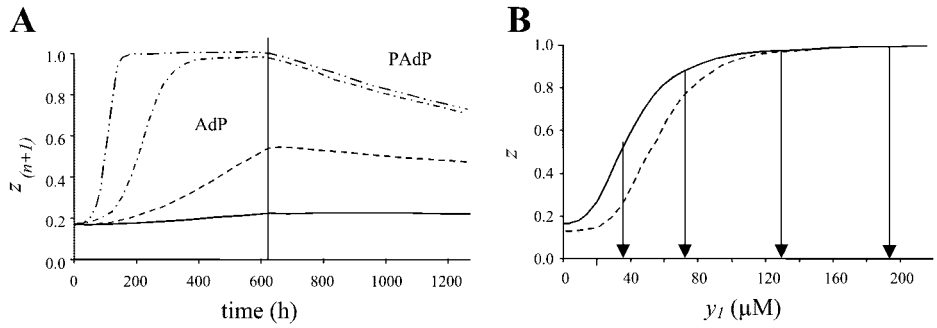

Fig. 6. Kinetic and dynamic behavior of *system 2* logistic variables. *A*: predictions, from *model L3*, of $z_{(n+1)}$ variations over experimental duration [during administration period (AdP) and after cessation of treatment (PAdP)] for the 4 oral Sr doses: D_1 (solid line), D_2 (dashed line), D_3 (dashed-dotted line), and D_4 (dashed-dotted-dotted line). *B*: computed dependence of the asymptotic value of $z_{(n+1)}$ (solid line) and $z_{(n+2)}$ (dashed line) on *compartment 1* Sr concentration. Vertical arrows, asymptotic *compartment 1* Sr concentration reached for each Sr dose. Each *z* variable is expressed in normalized concentration (defined in APPENDIX A).

total amount of mineral (Ca + Sr) incorporated into bone solid phase should be maintained in a range not significantly different, regardless of the increase in the *compartment 1* Sr concentration. Thus only the noncompetitive inhibition seems to be responsible for physicochemical discrimination against Sr. This is the case if the predicted apparent Ca and Sr concentrations in *compartment 3* are examined. Because of the difference between the Ca and Sr fractional transfers from *compartment 3* to *compartment 2* (λ_{23} vs. k_{23}), the relative concentration of Sr in bone surface *compartment 3* is higher than that of Ca (high Sr-to-Ca molar ratio for *compartment 3* in contrast to that of other compartments), a discrimination that is also predicted during Sr administration.

Other structural arrangements of the bone interfacial substructure (such as competitive, rather than noncompetitive, inhibition; see Fig. 12) cannot be ruled out, because they can produce model responses correctly fitting the experimental data. Interestingly, it was possible to refute the hypothesis that inhibition of the Langmuir process results from a simple competition between Ca and Sr for the same adsorption sites. We used the above model with *compartment 3* directly linked to *compartment 1* (as in the initial *model L3*; Fig. 1), eliminating the noncompetitive inhibition, but we could not identify parameter values that correctly fit the experimental data with reliable model behavior for Ca bone metabolism.

Finally, there is no reason to reject the simpler initial *models L3* and *L6*, even if the refined model, including an explicit representation of the interfacial dynamics of Sr alone, has an interesting heuristic potential and can be justified from a modeling point of view. Simple and refined models have quite similar overall properties. The mineral mass distributions and the predicted main transfer rates are essentially identical whatever the (time-implicit or time-explicit) formulation used for the Langmuir-type function. However, *model L3* appears to be better than *model L6*. It is indeed physiologically difficult to reconcile the high mineral mass of *compartment 6* to a dynamic behavior associated with the inhibition operating at the bone surface.

ENL Acting on G1 and/or Bone

It is necessary to analyze the characteristics of the time-explicit (differential) form of the logistic $z_{(n+1)}$ and $z_{(n+2)}$ variables that modulate a number of transfer rates inside our model (Fig. 1) and their nonlinear dependence on *compartment 1* Sr concentration (*Eqs. A4* and *A5*) for an understanding of their physiological meaning.

Kinetic and dynamic behavior of the logistic z variables. As reported for $z_{(n+1)}$ in *model L3* (Fig. 6*A*), the kinetic behavior of this variable reveals important differences between the various Sr doses. There is almost no change over time with the smallest dose (D_1), whereas $z_{(n+1)}$ increases acutely during oral Sr administration (AdP) with the highest one (D_4), to reach its maximum after ~40 h, with only slight changes. For the other two doses (D_2 and D_3), $z_{(n+1)}$ produced a more moderate change, intermediate between D_1 and D_4. During PAdP, $z_{(n+1)}$ tended to decrease at a rate that depended on the value reached at the end of AdP. The kinetics of $z_{(n+2)}$ (not shown) are rather similar to the kinetics of $z_{(n+1)}$, with some differences linked to distinctive parameter values (Table 2): the slopes of the

Table 2. *Model L3 parameters and initial conditions for system 2 logistic variables $z_{(n+1)}$ and $z_{(n+2)}$*

Parameter or Initial Condition	Value, dimension	CV, %
$g^1_{(n+1)0}$	9.61×10^{-04} $nC^{-1}\cdot h^{-1}$	62.5
$h_{0(n+1)}$	8.05×10^{-04} h^{-1}	63.1
$g^2_{(n+1)0}$	1.64×10^{-08} $nC^{-1}\cdot \mu M^{-p}\cdot h^{-1}$	53.4
$p_{(n+1)}$	2.94	3.97
$g^1_{(n+2)0}$	2.17×10^{-03} $nC^{-1}\cdot h^{-1}$	50.6
$h_{0(n+2)}$	1.90×10^{-03} h^{-1}	51.5
$g^2_{(n+2)0}$	5.35×10^{-10} $nC^{-1}\cdot \mu M^{-p}\cdot h^{-1}$	82.0
$p_{(n+2)}$	3.77	4.83
$z_{(n+1)}$ *(0)*	0.1621 nC_1	
$z_{(n+2)}$ *(0)*	0.1239 nC_2	

nC, normalized concentration; CV, coefficient of variation.

sharp rise during AdP and the fall during PAdP are more pronounced for $z_{(n+2)}$. From a dynamic point of view, the expected sigmoidal curves (Fig. 6*B*) obtained when the asymptotic z values (computed from the identified parameter values given in Table 2) are plotted against y_1 increasing values also differ according to whether $z_{(n+1)}$ or $z_{(n+2)}$ is considered, with concentrations for the half-maximal activating effect (HMC) slightly above 30 or 50 μM. These curves clearly indicate that the modulation of Sr metabolism (*system 1*) by the logistic z functions through their effects on the target FTF (K_{15}, K_{51}, and K_{21}) is not due to kinetic features alone but is also dose dependent. The asymptotic values of y_1 for the different Sr doses, i.e., the *compartment 1* values obtained after prolonged simulation of *model L3* with continued exogenous Sr, only gave the maximal increase (the z unit value) with the two highest doses for $z_{(n+1)}$ and $z_{(n+2)}$ (Fig. 6*B*). D_1 shows a smaller increment of $z_{(n+2)}$ than $z_{(n+1)}$.

Ca as an inducer of the z function: evidence for mineral self-regulation. Evidently, the high level of cooperativity revealed by the identified value of $p_{(n+1)}$ and $p_{(n+2)}$ (~3 and 4, respectively; Table 2), defining the order at which y_1 activates the z logistic functions, accounts for the main peculiarities reported above. Another interesting characteristic is that, despite showing large inaccuracy (Table 2), the identified values for $g^1_{(n+1)0}$ and $g^1_{(n+2)0}$, i.e., the constant parameters independent of y_1 in *Eq. A6*, have CV < 100%. Thus some organic and/or mineral species other than Sr and assumed to be constant throughout the experiment could influence the logistic functions. Inasmuch as Ca influences many cellular processes, we investigated whether the Sr dependence of extrinsic z functions could result from a direct interaction between Sr and Ca. We have merely conjectured that Sr mimics the inducing effects of Ca on some Ca^{2+}-dependent physiological processes. We changed the nonlinear *Eq. A6,* as shown in APPENDIX C, by *Eq. C1* to clarify the dependence of Ca and Sr on the z functions.

Equation C1 was applied to each of the z functions to determine whether this form was consistent with a model response fitting the experimental data and then to predict the link between the z functions and Ca concentrations, which would indicate a plausible mineral self-regulatory mechanism. With each *system 1* parameter maintained at a fixed value (that previously identified when the initial form of *Eq. A6* was used), the *system 2* parameters alone were estimated from *model L3*, with Y_1 = 1,250 μM, a constant value corresponding to the extracellular free Ca^{2+} concentration. Under such conditions, the model response correctly fit the experimental data. However, the a posteriori identifiability study showed an indetermination between the parameter values defining the Sr-to-Ca molar ratio efficiency [$g^3_{(n+1)0}$ and $g^3_{(n+2)0}$] and the cooperativity orders [$p_{(n+1)}$ and $p_{(n+2)}$]. Complete optimization was therefore performed with fixed $p_{(n+1)}$ and $p_{(n+2)}$ (5 and 6, respectively), chosen to be physiologically representative and slightly higher than the previously identified cooperativity orders (Table 2). A correct fit to data was obtained with CV < 100% for *system 2* parameter values. There were only minor variations of *system 1* parameter values that did not significantly differ from those previously identified. The dynamic behavior of the z logistic functions could be predicted through their theoretical dependence on not only Sr, but also Ca, concentration.

Hence, Sr and Ca activate the z logistic function; the S-shaped curves obtained with increasing Sr concentration have half-maximal concentrations of ~75 and 87 μM Sr for $z_{(n+1)}$ and $z_{(n+2)}$, respectively, in the absence of Ca (Fig. 7*A*). In the presence of physiological plasma Ca^{2+} concentration (1,250 μM), these curves were shifted toward lower Sr concentrations, with HMC close to 32 and 52 μM Sr, which are quite similar to the values obtained for *model L3* with the initial formulation of the ENL. Moreover, when the Ca dependence is investigated, the sigmoidal curves cover concentrations >25 times Sr concentration [Ca HMC of 2.2 and 3.1 mM for $z_{(n+1)}$ and $z_{(n+2)}$, respectively; Fig. 7*B*]. This finding agrees with the identified values of the Sr-to-Ca molar ratio [$g^3_{(n+1)0}$ and $g^3_{(n+2)0}$], which are ~30 for $z_{(n+1)}$ and 35 for $z_{(n+2)}$. This indicates that Sr is a better activator of the z logistic functions than Ca. However, this does not mean that Sr acts physiologically to induce such nonlinear functions. Although a "normal" Ca concentration influences Sr dependence (Fig. 7*A*), physiological Sr concentration (0.5 μM) does not change the predicted Ca dependence curves in Fig. 7*B*. Moreover, the Ca-response curves suggest that neither $z_{(n+1)}$ nor $z_{(n+2)}$ is sensitive to values close to, or lower than, the physiological extracellular Ca concentration. The maximal sensitivity to Ca is obtained at

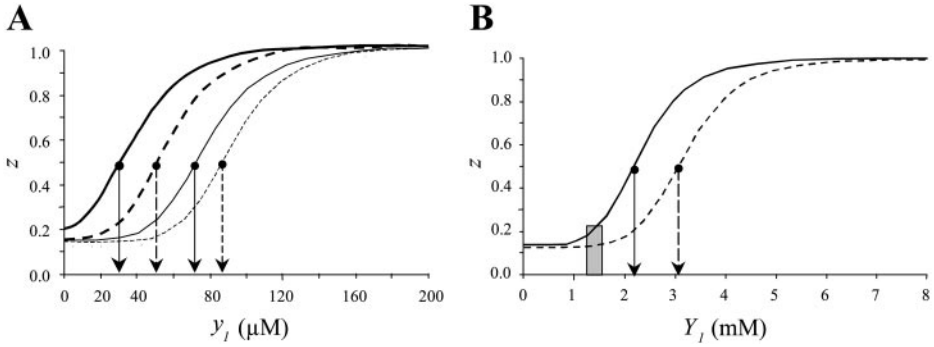

Fig. 7. Theoretical dependence of $z_{(n+1)}$ (solid line) and $z_{(n+2)}$ (dashed line) asymptotic value on Sr (*A*) and Ca (*B*) *compartment 1* concentration when Sr and Ca activate the z logistic functions. Arrows, half-maximal plasma mineral concentration for each computed curve. In *A*, thin and thick curves are obtained in the absence and presence, respectively, of a physiological plasma Ca concentration. In *B*, stippled vertical bar represents range of normal plasma free Ca concentration.

1.5–3.0 mM for $z_{(n+1)}$ and 2.2–4.0 mM for $z_{(n+2)}$ (Fig. 7*B*). This suggests that these functions operate only for Ca concentrations above the normal range.

Interaction Between INL and ENL: How Sr Affects Sr and Ca Metabolism

One of the peculiar features of the retained structure (*model L3*) is that it includes three nonlinear transfer functions, two of them combining INL and ENL (Fig. 1; see APPENDIX A). Indeed, in contrast to intestinal secretion, for which K_{51} is purely ENL [only $z_{(n+1)}$ in *Eq. A2*], K_{15} for the intestinal absorption and K_{21} for the influx of mineral from *compartment 1* to bone *compartment 2* result from mixing an M-M or a Langmuir-type equation with a z logistic function (*Eqs. A1* and *A3*). This intricacy gives rise to complex kinetic variations of these FTF, as predicted from the simulation of *model L3* during the experiment, depending on the Sr dose.

Time-varying FTF. Although variations in K_{51} only reflect variations of $z_{(n+1)}$ (Fig. 6*A*) with, for D_3 and D_4, a maximal increase during AdP of about six times its initial value, K_{21}, although modulated by the same logistic function [$z_{(n+1)}$], changes differently with time, with a maximum for D_4 of less than three times the initial value (Fig. 8*A*). This difference is due to the greater influence of the Langmuir-type than the logistic function: the Langmuir-type function tends to progressively decrease K_{21} when *compartment 3* (the inhibitory variable in *Eq. A3*) rises. Conversely, $z_{(n+1)}$ increases this FTF, but with its own y_1-dependent kinetics. K_{21} continuously decreases during AdP at the lowest Sr dose (Fig. 8*A*) because of the very small $z_{(n+1)}$ increment (Fig. 6*A*). In contrast, K_{21} increases sharply at the two highest doses, further counterbalanced by the opposite effect of the Langmuir-type nonlinearity. The relative weights of the nonlinearities are such that K_{21} for D_4 has a value that is lower than that for the intermediary D_2 and D_3 at the end of AdP. This could be interpreted as D_2 and D_3 being more efficient than D_4 for the transfer of mineral toward bone. This result could be important for the effect of Sr on Ca transfer to bone via bone formation/mineralization, because this metabolic process, characterized by K_{21}, is common to Ca and Sr, and the extracellular Ca concentration (Y_1) does not change significantly under our experimental conditions.

There are problems with the time variations of K_{15}, because the kinetic expressions of the INL (M-M) and ENL [$z_{(n+2)}$] do not match. Although $z_{(n+2)}$ is relatively slow, the M-M process depends on *compartment 5*, which has a high turnover rate and is directly influenced by the exogenous Sr. Hence, K_{15} varies over the short term and, thus, directly influences the comparison of the model response with the detailed plasma kinetic data collected during AdP (see Fig. 1 in Ref. 39). We use a value for K_{15} during AdP obtained just before the morning Sr dose, its maximal 24-h value, which fit the long-term kinetics of this FTF (Fig. 8*B*). The variations in K_{15} largely reflect those of the $z_{(n+2)}$ logistic function, with a highly nonlinear dose-dependent increase during AdP, followed by small changes during PAdP. However, the M-M INL also has an effect. First, K_{15} increases during the first part of PAdP, mainly for the two highest doses, as expected from the fast fall in *compartment 5* concentration resulting from the cessation of exogenous Sr. Second, K_{15} reaches lower values for D_4 than for D_3 during the last part of AdP, in agreement with the unexpected dose dependence of K_{21} (Fig. 8*A*). The mineral transfer from the GI compartment to *compartment 1* tends to become saturated (K_{15} diminishes), because the *compartment 5* concentration exceeds the k_{15}^3 value (*Eq. A1*). This also occurs when short-term variations in K_{15} are considered (Fig. 8*C*). Despite large variations linked to the effect of exogenous Sr on *compartment 5*, the K_{15} FTF associated with

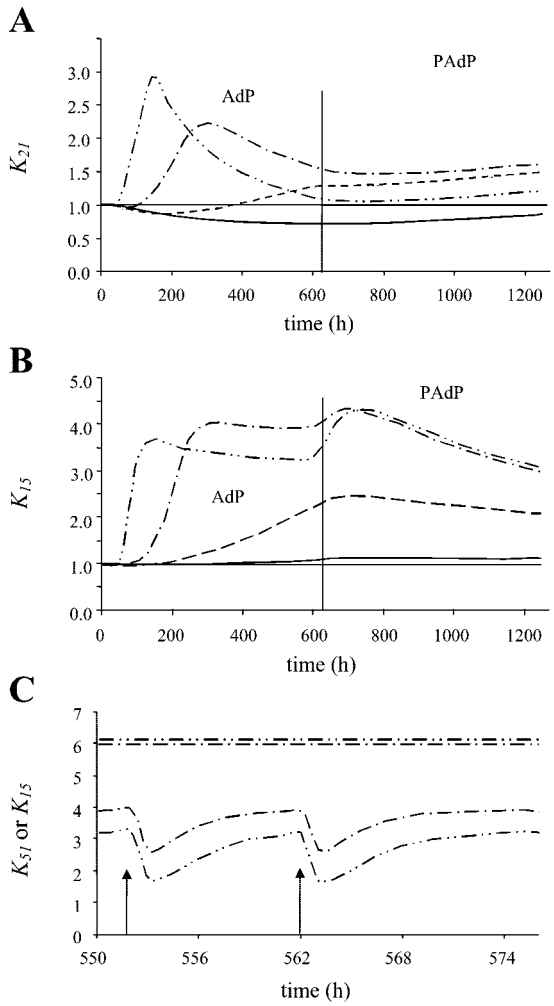

Fig. 8. Time variations of nonlinear fractional transfer functions predicted from *model L3* over experimental time (AdP and PAdP) for D_1–D_4 (see Fig. 1 legend for explanation of lines). *A*: complex kinetic behavior of mineral transfer from *compartment 1* to bone mineral solid phase, resulting, at K_{21} level, from interaction of a Langmuir-type intrinsic nonlinearity (INL) with a logistic extrinsic nonlinearity (ENL; see *Eq. A3*). *B* and *C*: because of the interaction of an M-M-type INL with a logistic ENL (see *Eq. A1*), K_{15} also has peculiar kinetics with complex dose-dependence relationship. *B*: long-term variations in K_{15}. *C*: short-term (24-h) kinetics for K_{15} compared with quasi-constant value of K_{51} (see *Eq. A2*) observed late in AdP for D_3 and D_4.

D_4 is always smaller than that for D_3 during the last part of AdP. Thus K_{15} varies daily between 1.7 and 3.2 times its initial value for D_4 and between 2.6 and 3.9 times its initial value for D_3. In addition, K_{51} remains nearly constant at about six times its initial value for D_4 and D_3. Globally, the dissimilarity between the dependence of $z_{(n+1)}$ and $z_{(n+2)}$ on y_1 (Fig. 6*B*) could be important for variations in the net mineral intestinal absorption capacity induced by Sr, in addition to the rather instantaneous effects of the M-M INL on K_{15}.

Dose-dependent effects of Sr on Ca metabolism. The above analysis has revealed an attractive property of the model related to the complex dose dependence of GI and bone FTF. If Sr and Ca share the same metabolic pathways, then the variations in FTF in response to exogenous Sr must also affect Ca metabolism. We have therefore departed from a strict physiological framework to examine the effects of exogenous Sr on the metabolism of Ca. The asymptotic behavior of the model variables was computed for Ca and Sr (see APPENDIX C) using different values for *compartment 1* Sr concentration (y_1) and a constant *compartment 1* Ca concentration (Y_1 = 2,500 μM) plus the set of parameter values previously identified from *model L3*.

Thus, for bone mineral metabolism, the inducing effect of Sr on the $z_{(n+1)}$ function and the Sr-specific inhibitory effect on the transfer of mineral from *compartment 1* to bone (K_{21}) through the Langmuir-type nonlinearity are taken into account. A range of Sr concentrations, y_1 = 30–110 μM (Fig. 9), were found, for which the asymptotic Ca mass in *compartment 6* (mineral solid phase associated with mature bone) is increased, with the assumption of no other interaction between Sr and Ca. The maximal effect is obtained for y_1 = 55 μM, with a 35% increase in bone Ca mass compared with that obtained at physiological Sr concentration. *Compartment 6* has an asymptotic value below the physiological value at other values of y_1. The Langmuir-type nonlinearity is indeed more efficient than the $z_{(n+1)}$ logistic function in two situations: when $y_1 < 30$ μM and there is only a small increase in $z_{(n+1)}$, and when $y_1 > 120$ μM and the Langmuir-type function continues to decrease the mineral transfer to bone while $z_{(n+1)}$ approaches its maximal unit value (Fig. 9).

Using a fixed value for each parameter with, for Ca, k_{01} (urinary excretion) divided by 2 and K_{51} divided by 16, we then applied the same theoretical procedure to GI metabolism (Fig. 2). The asymptotic steady state was computed by monitoring the mean daily Ca ingestion required to maintain the *compartment 1* Ca concentration constant (Y_1 = 2,500 μM), whatever the value of the Sr concentration (y_1). The changes induced by the K_{51} and K_{15} y_1 dependence through $z_{(n+1)}$ and $z_{(n+2)}$, together with the K_{15} M-M nonlinearity influence, caused intestinal mineral absorption capacity to vary, and this must be counterbalanced by the dietary Ca intake. The predicted values of the mean daily Ca ingestion as a function of y_1 are reported in Fig. 9*B*. The maximum value was ~1,200 mg/day for y_1 = 35 μM, with values lower than the initial value for $y_1 > 65$ μM. These values can be within a normal physiological range, despite the large dose-dependent increases in K_{51} and K_{15} related to the modulation by $z_{(n+1)}$ and $z_{(n+2)}$. Thus the Sr concentration that has the maximal effect on bone formation/mineralization (y_1 = 55 μM) requires only a small increment in the daily Ca intake. The required Ca intake, 989 mg/day, remains in the normal range and corresponds to only a 14% increase over the value (868 mg/day) computed using a physiological Sr concentration.

An integrative mechanism for intestinal secretion of endogenous mineral. Finally, we examined the bidirectionality of the relation of GI *compartment 5* to *compartment 1*. The satisfactory initial models (Fig. 1), as well as the refined GI compartmental structure with the intermediary intestinal cellular compartment explicitly considered (*compartment 1′* in Fig. 4), require reversibility between lumen and plasma. This kinetic reversibility could be due to peculiar features of some process involved in the facilitated membrane transport of mineral, as suggested for intestinal Ca absorption. Two mechanisms of Ca entry from the gut lumen into the enterocyte via the apical membrane have been proposed: the first mechanism may be essentially irreversible, with a Ca^{2+} channel similar to that recently detected in the proximal small intestine [mainly in the duodenum (19)]; the second mechanism, associated with a lipid-soluble mobile carrier, could be reversible to some extent (47). Each of these processes, channels (19), channel-like transporters (31), or mobile carriers (47), is also saturable, with an apparent M-M constant in the same range as that estimated by our model. Finally, multiple signaling pathways may regulate them, a property consistent with their modulation, in our model, by extrinsic z functions.

A satisfactory fit to experimental data is obtained only when the saturable part of the intestinal absorption and the endogenous secretion are modulated by

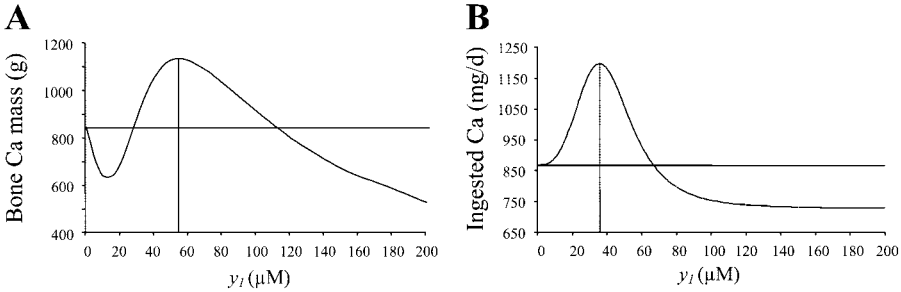

Fig. 9. Complex dose-dependent effect of Sr on GI and bone Ca metabolism according to *model L3*. *A*: asymptotic Ca mass in *compartment 6* (bulk bone solid phase) as a function of *compartment 1* Sr concentration. *B*: asymptotic oral Ca intake required to maintain *compartment 1* at physiological plasma Ca concentration (2.5 mM) as a function of *compartment 1* Sr concentration.

one distinct z function, as reported elsewhere (39). Hence, our model agrees with these two processes, which operate in opposite directions, involving different transport systems, which can be neither refuted nor supported because of uncertainty about the molecular mechanism(s) of intestinal endogenous secretion. Is this last process active, passive, hormonally dependent, or related to exsorption? However, another proposition is that part of the entering mineral may be reversible (reversible mobile carrier), so that Ca_i or intracellular Sr may be countertransported out of the cell to the intestinal lumen, in addition to an irreversible process (channel-dependent process). This was checked using a refined model. We assumed that two M-M equations operated simultaneously on the transfer from *compartment 5* to *compartment 1*, in addition to the nonsaturable part of intestinal absorption (paracellular transfer). Each M-M equation depended on one distinct extrinsic logistic function [$z_{(n+2)}$ or $z_{(n+3)}$], and we assumed $z_{(n+3)}$ modulating one M-M equation and also the mineral transfer from *compartment 1* to *compartment 5* (intestinal endogenous secretion). Obviously, there were many more unknown parameters (addition of 6 parameters and 1 *system 2* variable). Also, optimization was undertaken with numerous parameter values set at those identified for *model L3*; only the parameter values directly related to bone and GI nonlinear behaviors were reevaluated, with $p_{(n+1)}$ and $p_{(n+2)}$, respectively, the cooperativity order of the z functions acting, on the one hand, on bone and, on the other hand, on the GI irreversible M-M equation. These conditions gave a correct fit to experimental data (not significantly different from that obtained from *model L3*), even with the use of a reversible process accounting for a large part of the total saturable transfer. For instance, if the same maximal rate for reversible and irreversible parts of the saturable transfer under physiological conditions (at *time 0*) is assumed, the set of identified parameter values shows similar M-M constants that were also close to the corresponding value for the initial *model L3* (k_{15}^3 in *Eq. A3*). The main changes were in the S-shaped y_1 dependence curves computed for each z function (Fig. 10). Thus,

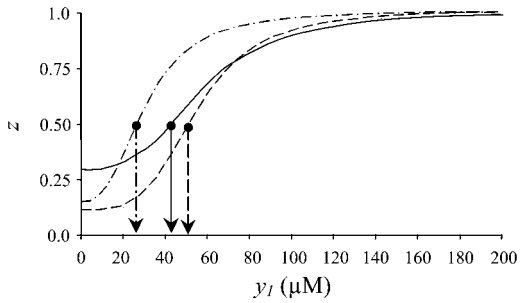

Fig. 10. Computed S-shaped curves of y_1 dependence for 3 logistic variables: $z_{(n+1)}$ (solid line), which modulates bone fractional transfer function, K_{21}; $z_{(n+2)}$ (dashed line), which modulates a first saturable irreversible process of intestinal Sr absorption; and $z_{(n+3)}$ (dashed-dotted line), which acts on another intestinal absorption process that is reversible because of modulation of intestinal endogenous mineral secretion by this same extrinsic $z_{(n+3)}$ variable.

contrary to the results in Fig. 6*B*, $z_{(n+1)}$ and $z_{(n+2)}$ differ more in the slope of the curve, which is smoother for $z_{(n+1)}$ than for $z_{(n+2)}$, than in their HMC values (~42 and 50 μM). Despite a slightly lower cooperativity order (2.62) for $z_{(n+3)}$ than for $z_{(n+1)}$ (2.96), the $z_{(n+3)}$ function modulating the reversible part of the intestinal absorption appears to be more sensitive to the *compartment 1* Sr concentration, with an HMC of ~25 μM.

The complexity of this model refinement precludes any other development in the absence of additional data for the GI compartment. Nevertheless, this apparent complexity might originate from the heterogeneity of the mineral absorption capacity along the intestine, which is not taken into account in our model (the single *compartment 5* includes all segments of the intestine that can transport mineral between lumen and blood; Fig. 1). For instance, the proximal part of the intestine (duodenum) could make a major contribution to the irreversible process, whereas the reversible component could be representative of the more distal segments (e.g., ileum) and, thus, be mostly responsible for the intestinal secretion of endogenous Sr and Ca (43).

DISCUSSION

The present study was prompted by the need to analyze the relevance of a nonlinear compartmental model, developed in the companion paper (39) to describe human Sr metabolism, for Ca metabolism. Given the model structure (Fig. 1) and the new quantitative and mainly qualitative information it offers, our purpose was to test the feasibility of physiological mechanisms that could underlie the nonlinear processes included in this model, with their intrinsic or extrinsic nature. Using model refinements, we were able to check a set of assumptions related to the origin of these nonlinearities and compare refined model predictions with the few available data concerning Ca metabolism under Sr supplementation. (Only data relative to total and free plasma Ca concentration and daily urinary Ca excretion were assessed over the experimental duration.) Of course, considering the theoretical and practical identifiability requirements, the refined structures were often overmodeled. Thus any refined model is only an illustration of a mechanistic hypothesis, rather than a fully justified step of modeling. Nevertheless, this approach has several advantages and seems to be of importance for a better understanding of Ca metabolism, its regulation, and the Ca-Sr discrimination (see below).

First, and as a necessary condition for further discussion, the relevance of the Sr model to Ca metabolism is supported by the overall agreement of the model predictions at the initial state, including discrimination of Ca over Sr. As it was for Sr metabolism (39) and under the assumption that the whole Sr or Ca metabolism is in an asymptotic steady state (zero net mineral bone balance), the quantitative characteristics of Ca metabolism predicted at *time 0* (under physiological conditions) are consistent with experimental results

for Ca mass distribution and the rates of the main metabolic pathways when, in addition to urinary excretion, some GI processes involved in the net mineral intestinal balance discriminate in favor of Ca. The estimated absorption of Ca is then ~1.5 times that of Sr, close to that reported in the literature (44). Thus these observations corroborate several published in vivo investigations.

Second, we take advantage of the peculiarities of our model and use its constitutive intrinsic intestinal and bone nonlinearities to examine the underlying mechanisms and the processes that may distinguish between Sr and Ca in the GI tract or bone. This kind of study was not possible for kidney mineral metabolism, because the rates of glomerular filtration/renal secretion and tubular reabsorption are too fast for our model. Consequently, the Sr-to-Ca ratio of urinary clearance, estimated to be ~2, in agreement with other evaluations (21), was used to account for the Sr-Ca discrimination during tubular reabsorption.

The GI compartmental substructure has two distinctive properties. *1*) Nonsaturable (linear, paracellular) and saturable (M-M type, transcellular) transport processes are clearly indicated and quantitatively identified from in vivo kinetic and dynamic (dose-dependent Sr kinetics) data. The parameter values for the Sr-saturable process (maximum velocity 21.6 mmol/day and M-M constant ~0.8 mM) are on the same order as those expected for physiological intestinal Ca transport, consistent with the idea that Sr and Ca intestinal absorption use similar transcellular paths (4, 42). Thus our results are at variance with the existence of Sr-specific processes for intestinal absorption or the suggestion that Sr absorption is entirely passive. Furthermore, this saturable process is comparable to the first step in transepithelial mineral transport, as illustrated in the refined model with an intermediary intracellular compartment between the intestinal lumen and extracellular fluids. This may be the rate-limiting apical mineral uptake by enterocytes that is mediated by a Ca channel (19) and/or a channel-like transporter (31) with a half-saturation concentration of 0.4–1 mM (14, 31), which is quite close to that estimated here. Thus, according to our model, the discrimination between Ca and Sr in the GI tract is not mainly due to this process. *2*) The GI compartmental substructure includes a bidirectional relation between the gut and plasma. This bidirectionality anticipates the intestinal secretion of endogenous Ca or Sr to be reabsorbed. This reabsorption is required to fit the Sr experimental data and is important, because, together with the absorption process per se, it determines the net intestinal balance. The secretion of endogenous mineral is predicted to be nonsaturable, at least for the experimental Sr concentrations, but can be regulated, because it depends on one of the *z* extrinsic functions. It is thus comparable with the transcellular process that may operate mainly in the distal intestine (43). There may be an intestinal carrier with the properties of a mobile carrier that could transport mineral reversibly from both sides of the apical membrane, as experimentally seen using Sr as an analog of Ca and showing that both minerals can be transported and apparently countertransported (47). Such a reversible carrier might be important for the intestinal secretion of endogenous Ca and Sr and the regulation of the net intestinal mineral balance (45). The refined GI model that explores this eventuality shows that a part of mineral entry into enterocytes could be reversible at a mechanistic level. In this context, the extrusion of Ca or Sr across the apical intestinal membrane as a source for the intestinal secretion might account for discrimination between Ca and Sr, if it is more specific for Sr than for Ca or if the concentration of free Sr^{2+} in the enterocyte is higher than the concentration of free Ca^{2+}. It is known that two major enterocyte proteins, the cytosolic Ca binding protein and the basolateral plasma ATP-dependent Ca pump, have a much greater affinity for Ca than for Sr (20, 32). So, as proposed by Wasserman (44) and supported by our refined model, the higher efficiency of Ca_i than of intracellular Sr homeostasis in intestinal epithelium could indirectly contribute to the preferential net intestinal absorption of Ca over Sr.

At the initial steady state, our Sr model can be applied to Ca metabolism without any discrimination in favor of Ca over Sr in the bone. This agrees with most of the in vivo studies using Sr and/or Ca radioactive tracers, under steady-state conditions for Ca and Sr metabolism, that show little skeletal discrimination (10). Nevertheless, this behavior seems to contradict in vitro physicochemical evidence indicating that the substitution/incorporation of Sr into the apatite lattice depends on the growth rate, perfection (24), and age (30) of the crystal or that Sr inhibits HA growth and dissolution (9). The behavior predicted from the refined model that attempts to represent the Langmuir-type nonlinearity as a process of mineral adsorption at the bone surface plus noncompetitive inhibition is significant. First, it illustrates the physicochemical mechanisms involved in the first steps of mineral incorporation into bone solid phase and thus helps clarify the dynamic properties of the bone liquid-solid interface. Second, it reveals the preferential movement of Ca from the bone surface toward the bulk bone solid phase. According to our study, the residence time in the bone surface is ~28 days for Sr and ≥10 times less for Ca. Such a discrepancy between Ca and Sr at the bone surface is predominantly revealed in the nonsteady-state situation (kinetic discrimination). In physicochemical terms, the schema is based on the adsorption of Ca^{2+} (and Sr^{2+}) at the bone surface followed by the formation of unstable primary solid entities [similar to the surface nuclei as building units for crystal growth (35)], which may be the source of ions for extracellular fluids or used to increase the mineral bulk bone solid phase. Third, this refined model suggests that there are few free adsorption sites under physiological conditions, most of them being occupied by Ca^{2+}, in accordance with the report of Groer and Marshall (16). Sr probably enters the bone solid phase as a foreign component of apatite via adsorption and subsequent solid solution formation (13)

and may, in this way, participate in the overall process of bone solid phase formation. Fourth, the model predicts that Sr^{2+} not only competes with Ca^{2+} at the adsorption sites but also inhibits the first step of mineralization by stabilizing the binding of mineral species containing Sr to adsorption sites, so forming a small mineral pool rich in Sr at the bone surface. This effect appears to be specific to Sr, in that Ca does not behave in the same way. There has been little discussion of the physiological significance of a small bone mineral pool rich in Sr at the liquid-solid bone interface, except for the suggestion by Lengemann (22) that the "selection against Sr in bone appears to occur at some point after the initial entry of Sr^{2+} into the bone and is associated with Sr^{2+} incorporation into a less labile form of bone mineral." Finally, our model predicts that, at least for some particular Sr extracellular concentration range, this inhibition of bone solid phase formation by Sr is favorably counterbalanced in vivo by the action of an extrinsic *z* function that probably activates osteoblastic lineage cells and bone formation (see just below).

The mechanistic interpretation of the intrinsic M-M and Langmuir-type nonlinearities discussed above must be considered in the more general context of the overall nonlinear behaviors of our model (Fig. 1). Indeed, the more interesting result of our modeling procedure is the characterization of time-explicitly formulated *z* variables operating at GI and bone levels and identified in the absence of any direct observation on the physical entities with which they could be compared. These distinctive *z* functions are mainly related to the dynamic information in our data, a single set of model parameter values being identified to fit the experimental kinetics due to four oral doses of Sr, considered simultaneously. As discussed below, these *z* nonlinear functions can be compared with controlling variables that are sensitive to extracellular Sr and/or Ca concentrations and act in feedback on GI and bone mineral metabolism.

First, we need to know what these *z* extrinsic variables may represent. With their own nonlinear characteristics (see APPENDIX A), they are involved in the expression of an inherently saturable process with a typical sigmoidal response that is well adapted to cellular functions as diverse as hormone secretion and cell proliferation and differentiation. They probably implicate the activities of particular cellular system(s) influenced by changes in Sr and/or Ca concentration. The effects may be local or systemic and act on cells involved in mineral metabolism, such as osteoblastic lineage cells for bone and enterocytes for the GI tract.

Second, we need to know what makes these functions sensitive to Sr and Ca. The peculiar dependence of the *z* variables on Sr, and probably on Ca, strongly suggests the involvement of Ca^{2+} (polyvalent cation)-sensing receptor(s) (CaR), with their known high degree of cooperativity for Ca and/or other cations (6, 37). These CaR proteins respond to polyvalent cations other than Ca, and the concentration producing a half-maximal effect may be higher or lower than that of Ca (mM). In some respects, under cover of the main hypothesis that Sr and Ca interact in an additive manner, our results indicate that Sr is 25 times more potent than Ca on the suggestive CaR. This finding agrees with experimental studies indicating that some mineral trace elements, e.g., Pb^{2+}, Cd^{2+}, and Co^{2+}, additively activate CaR and are more potent CaR agonists than Ca^{2+} (18, 37). However, this sensitivity is not sufficient for the physiological concentration of Sr to significantly modify the predicted response to Ca. Our findings also suggest that the CaR is functionally similar to, but distinct from, the PCaR, because Sr^{2+} is a less potent agonist than Ca^{2+} for this receptor (25). This is consistent with the finding that oral Sr has no effect on hormone secretion or renal function, which depends on PCaR activation (6).

Third, we also need to know in what context the regulatory role of these functions is operating. We believe that the extrinsic nonlinearities represent the expression of peculiar physiological Ca self-regulatory processes revealed via Sr^{2+} interactions with CaR. Kinetically, the variables assumed to be effective in controlling GI and bone metabolic paths have slow turnover rates, with a mean residence time of $\geq$10 days, and then may be operating in adaptive, rather than homeostatic, processes for Ca metabolism. Hence, direct (non-hormone-dependent) self-regulatory CaR-dependent processes could occur in the GI or bone cellular system, as proposed by Brown and Pollack (6). CaR have been identified in intestinal epithelial cells (8, 15) and in osteoblastic lineage cells (34, 48). These osteoblastic cells respond to high concentrations of extracellular Ca^{2+} (34) and Sr^{2+} (7) and possess an Al^{3+}-sensitive CaR different from PCaR (33).

Finally, the physiological interpretation of our model could help us understand the pharmacological effects of oral Sr and the potential of Sr in the treatment of osteoporosis (28). There seems to be a plasma Sr concentration (40–100 μM) at which the beneficial action of Sr on bone-forming cells surpasses its inhibitory physicochemical action. The predicted long-term effect of the maintenance of plasma Sr concentration at ~60 μM on bone mineral mass (Fig. 9) could be significant in managing the therapeutic effects of an oral Sr dose. A normal Ca net balance in the GI tract can be obtained with a rather high, but physiological, dietary Ca intake in conjunction with this optimal plasma Sr concentration. Of course, these estimations must be used with care, because they are asymptotic predictions that are justified only if the parameter values do not vary over the longer-term Sr administration.

APPENDIX A

The following equations characterize the FTF K_{15}, K_{51}, and K_{21} (see Fig. 1 for their location in the model), which include ENL (see *Eqs. A5* and *A6*), associated (K_{15} and K_{21}) or not associated (K_{51}) with an INL, as defined in previously (39).

The mineral transfer from GI *compartment 5* to IDP *compartment 1* (the mineral intestinal absorption) is represented by an M-M-type equation

$$K_{15} = k^1_{15} + \frac{k^2_{15} z_{(n+2)}}{k^3_{15} + y_5} \quad (A1)$$

where y_5 is mineral concentration of GI *compartment 5*, k^1_{15} is the linear nonsaturable part of the transfer process, $k^2_{15} z_{(n+2)}$ is the maximal velocity modulated by a time-explicit z function, and k^3_{15} is the concentration of the source *compartment 5* for which the transfer rate is half-maximal; this last parameter is also referred to as the M-M constant.

The fractional transfer process from IDP *compartment 1* to GI *compartment 5* is a simple linear (nonsaturable) process modulated by $z_{(n+1)}$

$$K_{51} = k_{51} z_{(n+1)} \quad (A2)$$

The mineral transfer from *compartment 1* to bone *compartment 2* combines an INL, a Langmuir-type equation, with an ENL, $z_{(n+1)}$, as given by

$$K_{21} = k^1_{21} z_{(n+1)} \left\{ 1 - \frac{y_b - y_b(0)}{k^2_{21} + [y_b - y_b(0)]} \right\} \quad (A3)$$

Equation A3 is derived from a more general equation

$$K_{21} = k^1_{21} z_{(n+1)} / [k^2_{21} (1 + y_b / k^3_{21}) + y_1] \quad (A4)$$

describing a saturable process dependent on the mineral concentration of the source *compartment 1*, associated with an inhibitory process dependent on a *compartment* y_b (*compartment 3* or *compartment 6,* depending on whether *model L3* or *model L6* was used) other than the source compartment. Only the inhibitory process [a function of the increase in y_b relative to its initial value $y_b(0)$ in *Eq. A3*] was characterized, because we were unable (as reported in Ref. 39) to identify any significant saturable response depending on the source *compartment 1*. In *Eq. A3,* maximal fractional transfer is defined as $k^1_{21} z_{(n+1)}$; k^2_{21} is the concentration variation of y_b for which the half-inhibitory effect is reached. $K_{21} = k^1_{21} z_{(n+1)}$ at *time 0*.

The two ENLs, expressed as time-explicit differential equations (*system 2* of the nonlinear compartmental formalism in Ref. 39), are relative to z variables not directly involved in the mineral metabolism itself (*system 1*) but depending on the mineral concentration in *compartment 1* and acting on some *system 1* FTF. Their general form, shown here for $z_{(n+1)}$, is as follows

$$\frac{dz_{(n+1)}}{dt} = G_{(n+1)0} - h_{0(n+1)} z_{(n+1)} \quad (A5)$$

with

$$G_{(n+1)0} = [g^1_{(n+1)0} + g^2_{(n+1)0} y_1^{(p_{(n+1)})}] z_{(n+1)} [1 - z_{(n+1)}] \quad (A6)$$

defining a growth function known as the logistic equation (40), here normalized for a unit maximal value and showing cooperative dependence on *compartment 1* mineral concentration (y_1) through the parameter $p_{(n+1)}$. The logistic $z_{(n+1)}$ is expressed in normalized concentration.

APPENDIX B

By analogy with the usual application of the M-M equation, the nonlinear compartmental formalism can be used to describe the catalyzed transformation of a substrate into a product via a catalyst-substrate complex (11). The scheme (Fig. 11*A*) includes *compartments 1, 2*, and *3*, the substrate, product, and intermediary complex, whereas *compartment (n+1)* is related to the free reaction sites, the concentration of which must be sufficiently low relative to the substrate concentration for them to be saturated. Thus, in reference to the general nonlinear compartmental formalism presented in the companion article (39), the set of differential equations encompasses two interdependent (extrinsically nonlinear) systems: *system 1,* related to intact, bound, and altered substrate (y_1, y_3, and y_2, respectively) and *system 2*, which describes only the kinetics of the free reaction sites, $z_{(n+1)}$. With the assumption of a first-order reaction between substrate and sites, the time-explicit equations are

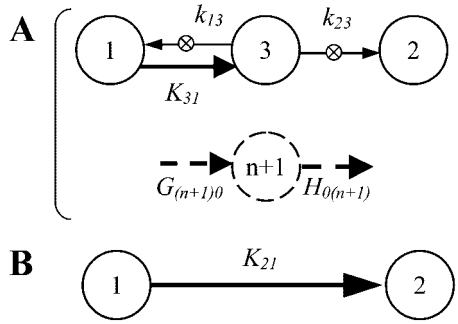

Fig. 11. Compartmental representation of an M-M-type reaction depending on whether there is (*B*) or is not (*A*) a pseudo-steady state [rapid equilibrium of intermediary step(s)]. *A*: *system 2 compartment (n+1)* represents an extrinsic z variable (free catalytic sites) involved in reversible formation of an intermediary species (*compartment 3*) from *compartment 1*. ⊗, Reaction associated with recovery of free sites, including the final step (formation of *compartment 2*) linearly dependent on *compartment 3* concentration. *B*: as soon as turnover between *compartment 1* and *compartment 3* is sufficiently high compared with fractional transfer from *compartment 3* to *compartment 2*, reaction can be simplified to *system 1* alone with an INL transfer function, K_{21}, described by the M-M equation. Such a compartmental representation can be applied to other mechanisms, such as transmembrane facilitated transport or adsorption of ions at the solid surface, possibly associated with physicochemical phase transition.

$$\left[\begin{aligned} \frac{dy_1}{dt} &= -K_{31} y_1 + k_{13} y_3 + \ldots \\ \frac{dy_2}{dt} &= k_{23} y_3 + \ldots \\ \frac{dy_3}{dt} &= K_{31} y_1 - (k_{13} + k_{23}) y_3 + \ldots \end{aligned} \right]$$

for *system 1* and

$$\frac{dz_{(n+1)}}{dt} = G_{(n+1)0} - H_{0(n+1)} z_{(n+1)} + \ldots$$

for *system 2*, with

$$K_{31} = k_{31} z_{(n+1)}$$
$$G_{(n+1)0} = (k_{13} + k_{23}) y_3$$
$$H_{0(n+1)} = k_{31} y_1$$

The system is in quasi-steady state when the equilibrium between substrate and the intermediary complex is rapidly compared with the product formation. A simple two-step reaction scheme gives a two-compartment (substrate and product) structure, including an M-M-type (time-implicit) INL (Fig. 11*B*)

$$\left[\begin{aligned} \frac{dy_1}{dt} &= -K_{21} y_1 + \ldots \\ \frac{dy_2}{dt} &= +K_{21} y_1 + \ldots \end{aligned} \right]$$

for *system 1*, with

$$K_{21} = \frac{k_{21}^1}{(k_{21}^2 + y_1)}$$

where k_{21}^1 defines the maximal reaction rate and k_{21}^2 is the substrate concentration at which the rate of transformation is half-maximal (M-M constant). The points of suspension indicate other possible metabolic routes for each of the variables. This kind of reaction was applied to the mineral intestinal absorption (carrier-facilitated transmembrane diffusion) by likening the intermediary *compartment 3* to the mineral/carrier complex and *compartment (n + 1)* to the free carrier.

Competitive, noncompetitive, or mixed inhibition (11) can be used with more complex schemes and more y variables (*system 1*). Such reaction schemes were used to show the first physicochemical steps in the transfer of mineral solute species to bone solid phase and to illustrate our interpretation of the Langmuir-type nonlinearity. This application was carried out for changes in physical states, rather than chemical transformations, as for the classical M-M equation. As illustrated in Fig. 12*A*, competitive inhibition occurs when two distinct substrates, e.g., *compartments 1* and *4*, compete for the same free sites $[z_{(n+1)}]$ with the formation of two different complex species, *compartments 3* and *5*. Noncompetitive inhibition (Fig. 12*B*) occurs with a single substrate (*compartment 1*) and with some of the substrate sites complex (*compartment 3*) removed, without recovery of free reaction sites, thus forming the second complex *compartment 4*. Finally, mixed inhibition is a complex combination of the two.

APPENDIX C

The applicability of models developed for Sr metabolism (from Sr kinetic data) to Ca metabolism was checked mainly by postulating that these minerals are similar enough that the metabolic processes for Sr are relevant to Ca. Inasmuch as we lacked adequate Ca kinetic data, we did not investigate the interactions between Ca and Sr at the kinetic level (except in 1 case; see below); we mostly examined the mass distribution of Ca and representative mineral fluxes after calculating the model asymptotic behavior using the physiological plasma Ca concentration, Y_1 = 2,500 or 1,250 μM, depending on whether total or free Ca^{2+} is considered. We questioned the calculated initial (*time 0*) steady state; if necessary, we looked for quantitative changes in parameter values to improve the model predictions. We also questioned the simulated effects of long-term oral Sr administration on Ca metabolism (see *Dose-dependent effects of Sr on Ca metabolism*).

Possible interaction between Ca and Sr involves the logistic z variables (defined by *Eqs. A5* and *A6*), which are highly cooperative in their dependence on the *compartment 1* Sr concentration. This should have a very significant physiological meaning if the underlying mechanisms were also Ca dependent. To show that this kind of nonlinearity can be formulated as dependent on Sr and Ca, *Eq. A6* was changed as follows

$$G_{(n+1)0} = \{g_{(n+1)0}^1 + g_{(n+1)0}^2 [Y_1 + g_{(n+1)0}^3 y_1]^{p_{(n+1)}}\} z_{(n+1)} \times [1 - z_{(n+1)}] \quad (C1)$$

where y_1 and Y_1 are the Sr and Ca concentrations in *compartment 1*, act with the same $p_{(n+1)}$ cooperativity order, and work in an additive manner (both minerals induce the z logistic function), except for the $g_{(n+1)0}^3$ factor, which defines the Sr-to-Ca molar ratio. Expressed in this way, it was possible to predict the dependence of the z variables on Sr and Ca concentration.

When the general form of the intrinsic Langmuir-type nonlinearity (*Eq. A4*) was expressed time explicitly, the consideration of Sr-dependent kinetics alone became somewhat ambiguous. Indeed, the saturable process dependent on the source *compartment 1* and the additional inhibition might be significantly influenced by variations in Sr and Ca concentrations. A dual set of differential equations corresponding to Sr (*system 1*) and Ca (*system I*) kinetics can be formulated. As an example, starting with the model structure given in Fig. 12*B* (without consideration of *compartment 2*) and assuming that Sr and Ca obey the same reaction scheme involving the free sites $z_{(n+1)}$ one obtains

$$\begin{bmatrix} dy_1/dt &= k_{13}y_3 - k_{31}z_{(n+1)}y_1 \\ dy_3/dt &= k_{31}z_{(n+1)}y_1 + k_{34}y_4 - (k_{13} + k_{23} + k_{43})y_3 \\ dy_4/dt &= k_{43}y_3 - k_{34}y_4 \end{bmatrix}$$

for *system 1* and

$$\begin{bmatrix} dY_1/dt &= \lambda_{13}Y_3 - \lambda_{31}z_{(n+1)}Y_1 \\ dY_3/dt &= \lambda_{31}z_{(n+1)}Y_1 + \lambda_{34}y_4 - (\lambda_{13} + \lambda_{23} + \lambda_{43})Y_3 \\ dY_4/dt &= \lambda_{43}Y_3 - \lambda_{34}Y_4 \end{bmatrix}$$

for *system I*, where each compartment of the structure is linked to the Sr concentration (y_i) and the Ca concentration (Y_i) and with Sr and Ca reacting as ligands for free sites separately from each other; then the single *system 2* becomes

$$dz_{(n+1)}/dt = (k_{13} + k_{23})y_3 - k_{31}z_{(n+1)}y_1 + (\lambda_{13} + \lambda_{23})Y_3 - \lambda_{31}z_{(n+1)}Y_1$$

thus the loss/recovery of the free sites depends on Sr and Ca. Note that k_{ij} and λ_{ij} differ only when there is discrimination

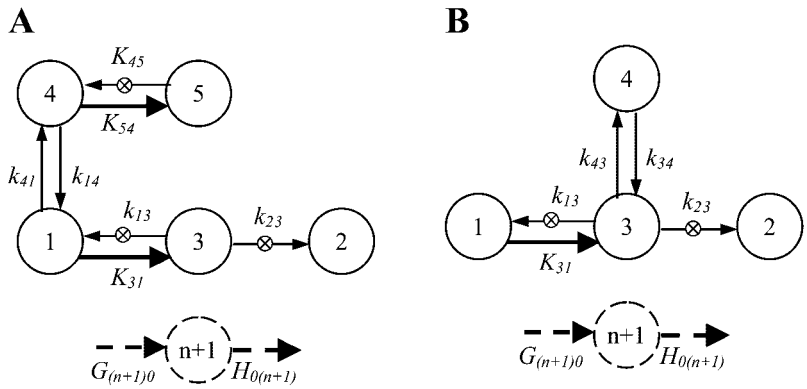

Fig. 12. Compartmental structures with explicit ENL (interaction between *systems 1* and *2*) and showing competitive (*A*) or noncompetitive (*B*) inhibition of the M-M-type reaction. *A*: 2 substrates (*compartments 1* and *4*) compete to form intermediary species (*compartments 3* and *5*). *B*: a first intermediary species is in reversible exchange with a second.

between Sr and Ca. Under such conditions, the model kinetic behavior can be simulated without neglecting the interactions between Sr and Ca, and numerical parameters can be estimated to show any difference between the two minerals.

The authors thank Dr. G. Milhaud for helpful discussions.

This study was supported by the Centre National de la Recherche Scientifique and the Institut de Recherches Internationales Servier.

REFERENCES

1. **Apfelbaum F, Mayer I, Rey C, and Labugle A.** Magnesium in maturing synthetic apatite: a Fourier-transformed infrared analysis. *J Crystal Growth* 144: 304–310, 1994.
2. **Blumenthal NC, Cosma V, and Levine S.** Effect of gallium on the in vitro formation, growth, and solubility of hydroxyapatite. *Calcif Tissue Int* 45: 81–87, 1989.
3. **Blumenthal NC and Posner AS.** In vitro model of aluminum-induced osteomalacia: inhibition of hydroxyapatite formation and growth. *Calcif Tissue Int* 36: 439–441, 1984.
4. **Blumsohn A, Morris B, and Eastell R.** Stable strontium absorption as a measure of intestinal calcium absorption: comparison with the double-radiotracer calcium absorption test. *Clin Sci Lond* 87: 363–368, 1994.
5. **Boivin G, Deloffre P, Perrat B, Panczer G, Boudeulle M, Mauras Y, Allain P, Tsouderos Y, and Meunier PJ.** Strontium distribution and interactions with bone mineral in monkey iliac bone after strontium salt (S12911) administration. *J Bone Miner Res* 11: 1302–1311, 1996.
6. **Brown EM and Pollack M.** The extracellular calcium-sensing receptor: its role in health and disease. *Annu Rev Med* 49: 15–29, 1998.
7. **Canalis E, Hott M, Deloffre P, Tsouderos Y, and Marie PJ.** The divalent strontium salt S12911 enhances bone cell replication and bone formation in vitro. *Bone* 18: 517–523, 1996.
8. **Chattopadhyay N, Cheng I, Rogers K, Riccardi D, Hall A, Diaz R, Hebert SC, Soybel DI, and Brown EM.** Identification and localization of extracellular Ca^{2+}-sensing receptor in rat intestine. *Am J Physiol Gastrointest Liver Physiol* 274: G122–G130, 1998.
9. **Christoffersen J, Christoffersen MR, Kolthoff N, and Bärenholdt O.** Effects of strontium ion on growth and dissolution of hydroxyapatite and on bone mineral detection. *Bone* 20: 47–54, 1997.
10. **Comar CL and Wasserman RH.** Strontium. In: *Mineral Metabolism: An Advanced Treatise,* edited by Comar CL and Bronner F. New York: Academic, 1964, vol. II, p. 523–572.
11. **Cornish-Bowden A.** *Fundamentals of Enzyme Kinetics*. London: Butterworths, 1981.
12. **Dahl SG, Allain P, Marie PJ, Mauras Y, Boivin G, Ammann P, Tsouderos Y, Delmas PD, and Christiansen C.** Incorporation and distribution of strontium in bone. *Bone* 28: 446–453, 2001.
13. **Davis JA, Fuller CC, and Cook AD.** A model for trace metal sorption processes at the calcite surface: adsorption of Cd^{2+} and subsequent solid solution formation. *Geochim Cosmochim Acta* 51: 1477–1490, 1987.
14. **Feher JJ.** Computer simulation of calcium transport mechanisms: application to the intestinal absorption of calcium. *Math Comput Modelling* 19: 135–160, 1994.
15. **Gama L, Baxendale-Cox LM, and Breitwieser GE.** Ca^{2+}-sensing receptors in intestinal epithelium. *Am J Physiol Cell Physiol* 273: C1168–C1175, 1997.
16. **Groer PG and Marshall JH.** Mechanism of calcium exchange at bone surfaces. *Calcif Tissue Res* 12: 175–192, 1973.
17. **Grynpas MD, Hamilton E, Cheung R, Tsouderos Y, Deloffre P, Hott M, and Marie PJ.** Strontium increases vertebral bone volume in rats at a low dose that does not induce detectable mineralization defect. *Bone* 18: 253–259, 1996.
18. **Handlogten ME, Shiraishi N, Awata H, Huang C, and Miller RT.** Extracellular Ca^{2+}-sensing receptor is a promiscuous divalent cation sensor that responds to lead. *Am J Physiol Renal Physiol* 279: F1083–F1091, 2000.
19. **Hoenderop JGJ, Hartog A, Stuiver M, Doucet A, Willems PHGM, and Bindels RJM.** Localization of the epithelial Ca^{2+} channel in rabbit kidney and intestine. *J Am Soc Nephrol* 11: 1171–1178, 2000.
20. **Ingersoll RJ and Wasserman RH.** Vitamin D-induced calcium-binding protein. Binding characteristics, conformational effects and other properties. *J Biol Chem* 246: 2808–2814, 1971.
21. **Leeuwenkamp OR, Van Der Vijgh WJF, Husken BCP, Lips P, and Netelenbos JC.** Human pharmacokinetics of orally administrated strontium. *Calcif Tissue Int* 47: 136–140, 1990.
22. **Lengemann FW.** Studies on the discrimination against strontium by bone grown in vitro. *J Biol Chem* 235: 1859–1862, 1960.
23. **Levine BS, Walling MW, and Coburn JW.** Intestinal absorption of calcium: its assessment, normal physiology and alterations in various disease states. In: *Disorders of Mineral Metabolism.* New York: Academic, 1982, vol. 2, p. 103–188.
24. **Likins RC, Posner AS, Paretzkin B, and Frost AP.** Effect of crystal growth on the comparative fixation of Sr^{89} and Ca^{45} by calcified tissues. *J Biol Chem* 236: 2804–2806, 1961.
25. **Mailland M, Waelchli R, Ruat M, Boddeke HGWM, and Seuwen K.** Stimulation of cell proliferation by Ca and a calcimimetic compound. *Endocrinology* 138: 3601–3605, 1997.
26. **Marie PJ, Garba MT, Hott M, and Miravet L.** Effect of low doses of stable strontium on bone metabolism in rats. *Miner Electrolyte Metab* 11: 5–13, 1985.
27. **Marshall JH, Liniecki J, Lloyd EL, Marotti G, Mays CW, Rundo J, Sissons HA, and Snyder WS.** Alkaline earth metabolism in adult man. *Health Phys* 24: 125–221, 1973.
28. **Meunier PJ, Solsman D, Delmas PD, Sebert JL, Albanese C, Brandi ML, Lorenc R, Beck-Jensen JE, Devernejoule NC, Proverdini DM, Tsouderos Y, and Register JY.** Strontium ranelate as a treatment of vertebral osteoporosis (Abstract). *J Bone Miner Res* 12 *Suppl* 1: S129, 1997.
29. **Missiaen L, Parys JB, Weidema AF, Sipma H, Vanlingen S, De Smet P, Callewaert G, and De Smedt H.** The bell-shaped dependence of the inositol 1,4,5-trisphosphate-induced Ca^{2+} release is modulated by Ca^{2+}/calmodulin. *J Biol Chem* 274: 13748–13751, 1999.
30. **Neuman WF, Gjornerstedt R, and Mulryan BJ.** Synthetic hydroxyapatite crystals. II. Aging and strontium incorporation. *Arch Biochem Biophys* 101: 215–224, 1963.
31. **Peng JB, Chen XZ, Berger UV, Vassilev PM, Tsukaguchi H, Brown E, and Hediger MA.** Molecular cloning and characterization of a channel-like transporter mediating intestinal calcium absorption. *J Biol Chem* 274: 22739–22746, 1999.
32. **Pfleger H and Wolf HU.** Activation of membrane-bound high-affinity calcium ion-sensitive adenosine triphosphatase of human erythrocytes by bivalent metal ions. *Biochem J* 147: 359–361, 1975.
33. **Pi M, Garner SC, Flannery P, Spurney RF, and Quarles LD.** Sensing of extracellular cations in CaSR-deficient osteoblasts. Evidence for a novel cation-sensing mechanism. *J Biol Chem* 275: 3256–3263, 2000.
34. **Quarles LD.** Cation sensing receptors in bone: a novel paradigm for regulating bone remodeling? *J Bone Miner Res* 12: 1971–1974, 1997.
35. **Randolph AD and Larson MA.** Crystallization kinetics. In: *Theory of Particulate Processes. Analysis and Techniques of Continuous Crystallization* (2nd ed.). New York: Academic, 1988, p. 109–134.
36. **Reeve J and Hesp R.** A model-independent comparison of the rates of uptake and short-term retention of ^{47}Ca and ^{85}Sr by the skeleton. *Calcif Tissue Res* 22: 183–189, 1976.
37. **Riccardi D.** Cell surface, Ca^{2+} (cation)-sensing receptor(s): one or many? *Cell Calcium* 26: 77–83, 1999.
38. **Slepchnenko BM and Bronner F.** Modeling of transcellular transport in rat duodenum points to coexistence of two mechanisms of apical entry. *Am J Physiol Cell Physiol* 281: C270–C281, 2001.
39. **Staub JF, Foos E, Courtin B, Jochemsen R, and Perault-Staub AM.** A nonlinear compartmental model of Sr metabolism.

I. Non-steady-state kinetics and model building. *Am J Physiol Regul Integr Comp Physiol* 284: R819–R834, 2003.
40. **Turner ME, Bradley EL, Kirk KA, and Pruitt KM.** A theory of growth. *Math Biosci* 29: 367–373, 1976.
41. **Vennekens R, Hoenderop JGJ, Prenen J, Stuiver M, Willems PHGM, Droogmans G, Nilius B, and Bindels RJM.** Permeation and gating properties of the novel epithelial Ca^{2+} channel. *J Biol Chem* 275: 3963–3969, 2000.
42. **Vezzoli G, Baragetti I, Zerbi S, Caumo A, Soldati L, Bellinzoni P, Centemero A, Rubinacci A, Moro G, and Bianchi G.** Strontium absorption and excretion in normocalciuric subjects: relation to calcium metabolism. *Clin Chem* 44: 586–590, 1998.
43. **Walling MW and Kimberg DV.** Calcium absorption or secretion by rat ileum in vitro: effects of dietary calcium intake. *Am J Physiol* 226: 1124–1130, 1974.
44. **Wasserman RH.** Strontium as a tracer for calcium in biological and clinical research. *Clin Chem* 44: 437–439, 1998.
45. **Wasserman RH and Fullmer CS.** Vitamin D and intestinal calcium transport: facts, speculations and hypotheses. *J Nutr* 125: 1971S–1979S, 1995.
46. **Williams RJP and Frausto da Silva JJR.** *The Natural Selection of the Chemical Elements*. Oxford, UK: Oxford University Press, 1996.
47. **Wilson HD, Schedl HP, and Christensen K.** Calcium uptake by brush-border membrane vesicles from the rat intestine. *Am J Physiol Renal Fluid Electrolyte Physiol* 257: F446–F453, 1989.
48. **Yamaguchi T, Chattopadhyay N, Kifor O, Ye C, Vassilev PM, Sanders JL, and Brown EM.** Expression of extracellular calcium-sensing receptor in human osteoblastic MG-63 cell line. *Am J Physiol Cell Physiol* 280: C382–C393, 2001.